Viscous regularization of strain localisation for softening materials

Eindhoven University of Technology

Viscous regularization of strain localisation for softening materials

Report WFW 93.090

M. G. D. GEERS

ir. **M.G.D. GEERS**
Eindhoven University of Technology
Faculty of Mechanical Engineering
June - July 1993

Viscous regularization of strain localisation for softening materials

1. Introduction

1.1. Strain localisation for softening materials

A large number of materials are characterised by a *softening* behaviour. These materials show a decrease of the load-carrying capacity when the limit load is exceeded. All deformations localise in finite small bands before fracture occurs. The corresponding conventional stress-strain diagram will show a descending branch (negative slope). This phenomenon is commonly called *strain softening* accompanied by *strain localisation*. The use of a strain-softening model in a classical continuum theory does not lead to hyperbolic field equations, describing the equilibrium of the material. The finite element solution converges to a localisation zone with zero thickness if the meshes refine. The solution becomes mesh-sensitive. (Needleman, 1988)

1.2. Aims of the study

In order to remedy the ill-posedness of the initial value problem for strain-softening models in classical continuum-formulations, many numerical techniques are recently developed. Several directions of avoiding the problem are advocated (de Borst 1992, Simo 1988, Sluys 1992):

- Using a rate dependent crack model
- Making the softening modulus dependent on element size
- Using a gradient dependent model (de Borst 1991)
- Viscoplastic regularization coupled with a physical scale dimension limiting the local defect size
- Using a Cosserat continuum model
- Using a nonlocal approach (Brekelmans 1993)
- Adaptive mesh-refinement, etc.

This study focuses on the viscous regularization of localisation by strain-softening to obtain a finite element formulation that is no longer mesh-sensitive. The localisation in narrow bands is examined, and the different results for progressively refined meshes are compared. The theoretical underlying approach is based on a viscous/creep damage-evolution law and Perzyna's viscoplastic model.

The analyses will be carried out under dynamic conditions, where inertia-effects will be taken into account (the wave propagation problem). Mode I and mode II-localisation are simulated by reflection of the loading-waves which causes the yield limit to be exceeded. On the other hand, a second analysis is performed, without wave propagation or inertia-contributions. In this case, small imperfections were used to obtain localisation. A brief discussion of the influence of an imperfection on the nature and width of the localisation zone is made.

To examine the failure by strain-localisation, two simple models are used, a two-dimensional tension bar and a one-dimensional shear layer. The influence of some model parameters is also evaluated. It is important to remark that this study only analyses the *numerical performance* of the presented viscous damage models, and does not really simulate experimentally measured data.

1.3. Outline of the study

The two viscous regularization techniques are theoretically described in Chapter 2. Paragraph 2.1 deals with the viscous damage model, while paragraph 2.2 treats of Perzyna's viscoplastic model

involving damage. The implementation in a finite element formulation is described in paragraph 2.3.

The numerical analyses that are carried out, are described in Chapter 3. The models are sketched and the corresponding results are discussed. The two-dimensional tension bar is treated in paragraph 3.1. Paragraph 3.1.1. treats of the dynamic approach including inertia-effects (wave propagation), while paragraph 3.1.2. deals with a quasi-static analysis without inertia-contributions. The shear layer model is analysed in paragraph 3.2.

The essential conclusions are summarised in Chapter 4.

2. Viscous regularization - the damage approach

Throughout the elaboration of the theoretical model tensor notations will be used to derive the constitutive relations.

2.1. The viscous damage evolution law

To describe the mechanical behaviour of strain-softening materials, an internal state variable, *the damage*, will be incorporated into the constitutive model (Kachanov 1986, Lemaitre and Chaboche 1990). The damage is assumed to be isotropic. Consequently the damage D will be a scalar variable. To incorporate this damage-variable in the constitutive model, the global elastic constitutive equation is modified as follows :

$$\boldsymbol{\sigma} = (1-D)\,{}^4\mathbf{D}_e : \boldsymbol{\varepsilon} \tag{2.1.1}$$

(${}^4\mathbf{D}_e$ being the elastic stiffness tensor, and D being the damage).
Assuming that at a time **t** the entire displacement field (and thus the total strain) and the current damage values are known, one can determine the stress tensor at time **t+Δt** for a given strain increment : $\boldsymbol{\sigma}^{t+\Delta t}$
One may then write $\Delta\boldsymbol{\sigma} = \boldsymbol{\sigma}^{t+\Delta t} - \boldsymbol{\sigma}^{t}$, where $\Delta\boldsymbol{\sigma}$ is depending on the state variables and the damage at time **t** , the incremental displacement field, the chosen time step and the model parameters.

Rewriting the global constitutive relation in a rate format :

$$\dot{\boldsymbol{\sigma}} = (1-D)\,{}^4\mathbf{D}_e : \dot{\boldsymbol{\varepsilon}} - \dot{D}\,{}^4\mathbf{D}_e : \boldsymbol{\varepsilon}$$

which in its incremental linearised form (second order terms neglected) gives :

$$\begin{aligned}
\Delta\boldsymbol{\sigma} &= (1-D^{t+\Delta t})\,{}^4\mathbf{D}_e : \boldsymbol{\varepsilon}^{t+\Delta t} - (1-D^{t})\,{}^4\mathbf{D}_e : \boldsymbol{\varepsilon}^{t} \\
\Delta\boldsymbol{\sigma} &= (1-D^{t}-\Delta D)\,{}^4\mathbf{D}_e : (\boldsymbol{\varepsilon}^{t} + \Delta\boldsymbol{\varepsilon}) - (1-D^{t})\,{}^4\mathbf{D}_e : \boldsymbol{\varepsilon}^{t} \\
\Delta\boldsymbol{\sigma} &= (1-D^{t}-\Delta D)\,{}^4\mathbf{D}_e : \Delta\boldsymbol{\varepsilon} - \Delta D\,{}^4\mathbf{D}_e : \boldsymbol{\varepsilon}^{t}
\end{aligned} \tag{2.1.2}$$

$$\Delta D = \int_t^{t+\Delta t} \dot{D}\,\mathrm{d}t$$

ΔD is calculated by means of an Euler forward prediction giving :

$$\Delta D = \dot{D}^t.\Delta t \qquad \text{where } \dot{D}^t = \left[\left\langle \frac{J(\mathbf{S})}{K(1-D)} - C \right\rangle\right]^r \tag{2.1.3.}$$

The damage evolution law used in this model is based on the creep damage evolution law from Kachanov (Kachanov 1986), where the parameter C is added. C represents a threshold value for damage initiation and evolution. The model parameters K and C fully control the viscous (or creep) character of the evolution law. Damage increments are calculated explicitly to simplify the equations to solve. An implicit damage scheme would introduce a non-symmetric tangential

stiffness tensor on this level and a system of equations in the next paragraph that would become quadratic. The drawback of this choice is a restriction on the time step that is used to integrate the differential equations.

$$\left[\frac{{}^4\mathbf{D}_e^{-1}}{1-D^t-\Delta D}\right]:\Delta\sigma = \Delta\varepsilon - \frac{\varepsilon^t}{1-D^t-\Delta D}\Delta D$$

The non-linear tangential stiffness tensor then becomes :

$${}^4\mathbf{D}_c{}^t = (1-D^t-\Delta D)\,{}^4\mathbf{D}_e$$

$$\Delta\sigma = {}^4\mathbf{D}_c{}^t:\Delta\varepsilon - \Delta\mathbf{q} \qquad \text{with } \Delta\mathbf{q} = {}^4\mathbf{D}_c{}^t:\left[\frac{\varepsilon^t}{1-D^t-\Delta D}\Delta D\right]$$

2.2. Perzyna's constitutive model for viscoplasticity

During an infinitesimal increment of stress, changes of strain are assumed to be composed of an elastic and a plastic part . The total strain rate can then be decomposed as follows :

$$\dot{\varepsilon} = \dot{\varepsilon}_e + \dot{\varepsilon}_{vp}$$

Analogous to the previous paragraph one has $\Delta\sigma = \sigma^{t+\Delta t} - \sigma^t$, where $\Delta\sigma$ is supplementary depending on the viscoplastic strain field. The viscoplastic strain rate in the Perzyna model (Perzyna 1966,1971, Timmermans 1991) for associative plastic flow is given by :

$$\dot{\varepsilon}_{vp} = \gamma\,\phi(f)\frac{\partial f}{\partial\sigma}$$

where f stands for the chosen yield function, and where γ stands for a viscous material model parameter

The Von Mises yield function $f = \frac{J(\mathbf{S})}{1-D} - \kappa$ will be used to describe the yield surface. $J(\mathbf{S})$ represents the equivalent stress and $\mathbf{S}$ the stress deviator, while κ represents the yield limit. The yield function and the viscoplastic strain rate depend on the current damage value D and the stress tensor σ . The function $\phi(f)$ will here be chosen as $(f/\kappa)^N$ where N is a material model parameter to fit experimental data. The global constitutive equation then becomes :

$$\sigma = (1-D)\,{}^4\mathbf{D}_e:(\varepsilon-\varepsilon_{vp})$$

Rewriting the global constitutive relation in a rate format :

$$\dot{\boldsymbol{\sigma}} = (1-D)\,{}^4\mathbf{D}_e:(\dot{\boldsymbol{\varepsilon}}-\dot{\boldsymbol{\varepsilon}}_{vp}) - {}^4\mathbf{D}_e:(\boldsymbol{\varepsilon}-\boldsymbol{\varepsilon}_{vp})\dot{D}$$

which in its incremental linearised form gives :

$$\Delta\boldsymbol{\sigma} = (1-D^t-\Delta D)\,{}^4\mathbf{D}_e:(\boldsymbol{\varepsilon}^t+\Delta\boldsymbol{\varepsilon}-\boldsymbol{\varepsilon}^t_{vp}-\Delta\boldsymbol{\varepsilon}_{vp}) - (1-D^t)\,{}^4\mathbf{D}_e:(\boldsymbol{\varepsilon}^t-\boldsymbol{\varepsilon}^t_{vp})$$

$$\Delta\boldsymbol{\sigma} = (1-D^t-\Delta D)\,{}^4\mathbf{D}_e:(\Delta\boldsymbol{\varepsilon}-\Delta\boldsymbol{\varepsilon}_{vp}) - \Delta D\,{}^4\mathbf{D}_e:(\boldsymbol{\varepsilon}^t-\boldsymbol{\varepsilon}^t_{vp}) \qquad (2.2.1)$$

The incremental viscoplastic strain can be determined by means of an interpolation-parameter θ according to the chosen integration scheme ($\theta = 0$ explicit ; $\theta \neq 0$ implicit).

$$\Delta\boldsymbol{\varepsilon}_{vp} = \left[(1-\theta)\dot{\boldsymbol{\varepsilon}}^t_{vp} + \theta\,\dot{\boldsymbol{\varepsilon}}^{t+\Delta t}_{vp}\right]\Delta t \qquad (2.2.2)$$

$$\dot{\boldsymbol{\varepsilon}}^{t+\Delta t}_{vp} = \dot{\boldsymbol{\varepsilon}}^t_{vp} + \left[\frac{\partial\dot{\boldsymbol{\varepsilon}}_{vp}}{\partial\boldsymbol{\sigma}}\right]^t:\Delta\boldsymbol{\sigma} + \left[\frac{\partial\dot{\boldsymbol{\varepsilon}}_{vp}}{\partial D}\right]^t\Delta D \qquad (2.2.3)$$

Define ${}^4\mathbf{R} = \dfrac{\partial\dot{\boldsymbol{\varepsilon}}_{vp}}{\partial\boldsymbol{\sigma}}$

$$= \gamma\left[\frac{\partial\phi}{\partial f}\frac{\partial f}{\partial\boldsymbol{\sigma}}\frac{\partial f}{\partial\boldsymbol{\sigma}} + \phi\frac{\partial^2 f}{\partial\boldsymbol{\sigma}^2}\right]$$

Elaboration of ${}^4\mathbf{R}$ for the Von Mises yield function

$$f = \frac{J(\mathbf{S})}{1-D} - \kappa$$

$$= \frac{\sqrt{3\,J_2}}{1-D} - \kappa \quad \text{where } J_2 = \frac{1}{2}\mathbf{S}:\mathbf{S} \quad \text{with } \mathbf{S} = \boldsymbol{\sigma} - \frac{1}{3}\mathrm{tr}(\boldsymbol{\sigma})\mathbf{I}$$

$$\frac{\partial f}{\partial\boldsymbol{\sigma}} = \frac{\partial f}{\partial\mathbf{S}}:\frac{\partial\mathbf{S}}{\partial\boldsymbol{\sigma}}$$

$$\frac{\partial f}{\partial\mathbf{S}} = \frac{1}{1-D}\frac{\partial J(\mathbf{S})}{\partial\mathbf{S}} = \frac{1}{1-D}\frac{1}{2J(\mathbf{S})}\frac{3}{2}2\mathbf{S} = \frac{3\mathbf{S}}{2(1-D)J(\mathbf{S})}$$

$$\frac{\partial\mathbf{S}}{\partial\boldsymbol{\sigma}} = {}^4\mathbf{I} - \frac{1}{3}\mathbf{II}$$

$$\frac{\partial f}{\partial \sigma} = \frac{3\mathbf{S}}{2(1-D)J(\mathbf{S})} \qquad (\mathrm{tr}(\mathbf{S})=0)$$

$$\frac{\partial^2 f}{\partial^2 \sigma} = \frac{1}{1-D}\left[\frac{3\mathbf{S}}{2}\frac{-1}{J(\mathbf{S})^2}\frac{3}{2}\frac{\mathbf{S}}{J(\mathbf{S})} + \frac{3}{2J(\mathbf{S})}({}^4\mathbf{I} - \frac{1}{3}\mathbf{II})\right]$$

$$= \left[\frac{(D-1)}{J(\mathbf{S})}\frac{\partial f}{\partial \sigma}\frac{\partial f}{\partial \sigma} + \frac{3}{2(1-D)J(\mathbf{S})}({}^4\mathbf{I} - \frac{1}{3}\mathbf{II})\right]$$

$$\Rightarrow {}^4\mathbf{R} = \gamma\left[\frac{\partial \phi}{\partial f}\frac{\partial f}{\partial \sigma}\frac{\partial f}{\partial \sigma} + \frac{\phi}{J(\mathbf{S})}\left(\frac{3}{2(1-D)}({}^4\mathbf{I} - \frac{1}{3}\mathbf{II}) + (D-1)\frac{\partial f}{\partial \sigma}\frac{\partial f}{\partial \sigma}\right)\right]$$

define ${}^4\mathbf{M} = \frac{3}{2}({}^4\mathbf{I} - \frac{1}{3}\mathbf{II})$

$$\frac{\partial \phi}{\partial f} = N f^{N-1}$$

$$\Rightarrow {}^4\mathbf{R} = \gamma\left[N f^{N-1}\frac{\partial f}{\partial \sigma}\frac{\partial f}{\partial \sigma} + \frac{f^N}{J(\mathbf{S})(1-D)}\left({}^4\mathbf{M} - (1-D)^2\frac{\partial f}{\partial \sigma}\frac{\partial f}{\partial \sigma}\right)\right] \qquad (2.2.4)$$

$$\frac{\partial \dot{\varepsilon}_{vp}}{\partial D} = \frac{\partial(\gamma \phi \frac{\partial f}{\partial \sigma})}{\partial D} = \gamma\frac{\partial\left[\left(\frac{J(\mathbf{S})}{1-D} - \kappa\right)^N \frac{3\mathbf{S}}{(1-D)2J(\mathbf{S})}\right]}{\partial D}$$

$$= \gamma\frac{3\mathbf{S}}{2J(\mathbf{S})}\frac{\partial\left[\left(\frac{J(\mathbf{S})}{1-D} - \kappa\right)^N \frac{1}{(1-D)}\right]}{\partial D}$$

$$= \frac{\gamma 3\mathbf{S}}{2J(\mathbf{S})}\left[N\left(\frac{J(\mathbf{S})}{1-D} - \kappa\right)^{N-1}\frac{J(\mathbf{S})}{(1-D)^2}\frac{1}{1-D} + \left(\frac{J(\mathbf{S})}{1-D} - \kappa\right)^N \frac{1}{(1-D)^2}\right] = \mathbf{Z} \qquad (2.2.5)$$

ΔD is calculated in the same manner as outlined in the previous paragraph. To evaluate the balance between the implicit scheme of the viscoplastic strain and the explicit damage scheme, numeric iterative controls are performed to justify this approximation. The accuracy is found to be very good.

Substituting the equations (2.2.4) and (2.2.5) into equation (2.2.3) :

$$\dot{\varepsilon}_{vp}^{t+\Delta t} = \dot{\varepsilon}_{vp}^{t} + {}^4\mathbf{R} : \Delta\sigma + \mathbf{Z}\Delta D \qquad (2.2.6)$$

Rewriting (2.2.2), using (2.2.6) gives :

$$\Delta\boldsymbol{\varepsilon}_{vp} = \left(\dot{\boldsymbol{\varepsilon}}^{t}_{vp} + \theta\,{}^{4}\mathbf{R}:\Delta\boldsymbol{\sigma} + \theta\,\mathbf{z}\Delta D\right)\Delta t \qquad (2.2.7)$$

Substituting (2.2.7) in (2.2.1) :

$$\Delta\boldsymbol{\sigma} = (1-D^{t}-\Delta D)\,{}^{4}\mathbf{D}_{e}:(\Delta\boldsymbol{\varepsilon} - \dot{\boldsymbol{\varepsilon}}^{t}_{vp}\Delta t - \theta\,{}^{4}\mathbf{R}:\Delta\boldsymbol{\sigma}\,\Delta t - \theta\,\mathbf{z}\Delta D\,\Delta t) - {}^{4}\mathbf{D}_{e}:(\boldsymbol{\varepsilon}^{t} - \boldsymbol{\varepsilon}^{t}_{vp})\,\Delta D$$

$$\left[\frac{{}^{4}\mathbf{D}_{e}^{-1}}{1-D^{t}-\Delta D} + \theta\,{}^{4}\mathbf{R}\Delta t\right]:\Delta\boldsymbol{\sigma} = \Delta\boldsymbol{\varepsilon} - \dot{\boldsymbol{\varepsilon}}^{t}_{vp}\Delta t - \theta\,\mathbf{z}\Delta D\,\Delta t - \frac{(\boldsymbol{\varepsilon}^{t} - \boldsymbol{\varepsilon}^{t}_{vp})}{1-D^{t}-\Delta D}\Delta D$$

$${}^{4}\mathbf{D}_{c}^{\,t} = \left[\frac{{}^{4}\mathbf{D}_{e}^{-1}}{1-D^{t}-\Delta D} + \theta\,{}^{4}\mathbf{R}\Delta t\right]^{-1}$$

$$\Delta\boldsymbol{\sigma} = {}^{4}\mathbf{D}_{c}^{\,t}:\Delta\boldsymbol{\varepsilon} - \Delta\mathbf{q} \qquad \text{with } \Delta\mathbf{q} = {}^{4}\mathbf{D}_{c}^{\,t}:\left[\dot{\boldsymbol{\varepsilon}}^{t}_{vp}\Delta t + \theta\,\mathbf{z}\Delta D\,\Delta t + \frac{(\boldsymbol{\varepsilon}^{t} - \boldsymbol{\varepsilon}^{t}_{vp})}{1-D^{t}-\Delta D}\Delta D\right]$$

The incremental stress tensor and the new tangential stiffness tensor will be used in a finite element formulation in the next paragraph.

One can easily verify that the viscous damage model is fully incorporated in the extended model presented above.

2.3. Implementation in a finite element formulation

To implement the viscoplastic constitutive model (or the viscous damage model which is a part of it) in a finite element model, we shall now use the matrix-vector notation. concisely

2.3.1. The dynamic problem - wave propagation

The spatially discretised equation of motion describing the balance of momentum at time $t+\Delta t$ is given by the concisely written version of

$$\underset{\sim}{M}\,\ddot{\underset{\sim}{a}}^{t+\Delta t} = \underset{\sim}{f}^{t+\Delta t}_{ext} - \underset{\sim}{f}^{t+\Delta t}_{int} \quad \text{or}$$

$$\int_V \underline{H}^T \rho \underline{H} \tilde{\ddot{a}}^{t+\Delta t} dV = \tilde{f}_{ext}^{t+\Delta t} - \int_V \underline{B}^T \tilde{\sigma}^{t+\Delta t} dV \qquad (2.3.1)$$

in which $\tilde{\ddot{a}}^{t+\Delta t}$ is the acceleration array at time t+Δt
$\tilde{\sigma}^{t+\Delta t}$ is the stress array at time t+Δt
$\underline{H}$ is the matrix containing the interpolation polynomials
ρ is the density
$\underline{B}$ is the strain-nodal displacement matrix
($\underline{B} = \underline{L}\underline{H}$ with $\underline{L}$ the differential operator matrix)
$\tilde{f}_{ext}^{t+\Delta t}$ is the external load array at time t+Δt
$\tilde{f}_{int}^{t+\Delta t}$ is the internal force array at time t+Δt

To determine $\int_V \underline{B}^T \tilde{\sigma}^{t+\Delta t} dV$ an Euler forward method is used

$$\int_V \underline{B}^T \tilde{\sigma}^{t+\Delta t} dV = \int_V \underline{B}^T \tilde{\sigma}^{t} dV + \int_V \int_t^{t+\Delta t} \underline{B}^T \tilde{\dot{\sigma}} dt\, dV = \tilde{f}_{int}^{t} + \int_V \int_t^{t+\Delta t} \underline{B}^T \tilde{\dot{\sigma}} dt\, dV \qquad (2.3.2)$$

$\int_V \int_t^{t+\Delta t} \underline{B}^T \tilde{\dot{\sigma}} dt\, dV$ is evaluated introducing the incremental stress vector

$$\int_V \int_t^{t+\Delta t} \underline{B}^T \tilde{\dot{\sigma}} dt\, dV = \int_V \underline{B}^T \Delta\tilde{\sigma}\, dV$$

The incremental stress array is derived from the viscoplastic constitutive model as elaborated in the previous paragraph :

$$\Delta\tilde{\sigma} = \underline{D_c}^t \Delta\tilde{\varepsilon} - \Delta\tilde{q} = \underline{D_c}^t \underline{B} \Delta\tilde{a} - \Delta\tilde{q}$$

$$\int_V \underline{B}^T \Delta\tilde{\sigma} dV = \int_V \underline{B}^T \underline{D_c^t} \underline{B} \Delta\tilde{a} dV - \int_V \underline{B}^T \Delta\tilde{q} dV \qquad (2.3.3)$$

where $\Delta\tilde{a}$ stands for the incremental displacement array
Substituting (2.3.2) and (2.3.3) in (2.3.1) yields

$$\underline{M}\tilde{\ddot{a}}^{t+\Delta t} = \tilde{f}_{ext}^{t+\Delta t} - \tilde{f}_{int}^{t} - \int_V \underline{B}^T \underline{D_c^t} \underline{B} \Delta\tilde{a} dV + \int_V \underline{B}^T \Delta\tilde{q} dV$$

or

$$\underline{M}\tilde{\ddot{a}}^{t+\Delta t} = \tilde{f}_{ext}^{t+\Delta t} - \tilde{f}_{int}^{t} - \underline{K}^t \Delta\tilde{a} + \int_V \underline{B}^T \Delta\tilde{q} dV \qquad (2.3.4)$$

where $\underline{K}^t$ stands for the global stiffness matrix $\underline{K}^t = \int_V \underline{B}^T \underline{D_c^t} \underline{B}\, dV$

A direct time integration method using an implicit time integrator is used to obtain a fully discrete equation of motion. Assuming that the acceleration varies linearly over the time step, the following Newmark time integration scheme is used :

$$\begin{aligned} \dot{\underset{\sim}{a}}^{t+\Delta t} &= \dot{\underset{\sim}{a}}^{t} + \left[(1-\alpha)\ddot{\underset{\sim}{a}}^{t} + \alpha \ddot{\underset{\sim}{a}}^{t+\Delta t}\right]\Delta t \\ \underset{\sim}{a}^{t+\Delta t} &= \underset{\sim}{a}^{t} + \dot{\underset{\sim}{a}}^{t}\Delta t + \left[(\frac{1}{2}-\beta)\ddot{\underset{\sim}{a}}^{t} + \beta \ddot{\underset{\sim}{a}}^{t+\Delta t}\right]\Delta t^2 \end{aligned} \qquad (2.3.5)$$

where α and β are the Newmark integration parameters.

Equation (2.3.5) together with equation (2.3.4) results in a system of equations where $\underset{\sim}{a}^{t+\Delta t}$ $\dot{\underset{\sim}{a}}^{t+\Delta t}$ $\ddot{\underset{\sim}{a}}^{t+\Delta t}$ are the unknown variables to be determined. This system can be solved if the initial and boundary conditions are specified (Sluys 1992).
The dynamic Shock module of the DIANA finite element program is used to perform the Newmark time integration.

2.3.2. Implementation without inertia-effects

In this case, equation (2.3.4) can be readily transformed into the following equation :

$$\underset{\sim ext}{f}^{t+\Delta t} = \underset{\sim int}{f}^{t} + \underline{K}^{t}\,\Delta \underset{\sim}{a} - \int_V \underline{B}^{T}\,\Delta \underset{\sim}{q}\,dV$$

which can be easily implemented in a classical non-linear formulation.

2.3.3. Integration parameters - remarks

It is important to remark that the chosen integration scheme results in a tangential stiffness matrix that remains symmetric. The gain in accuracy that would be achieved by using more complicated schemes would render the system of equations to calculate $\Delta\sigma$ non-linear with a non-symmetric tangential stiffness matrix. The time needed to solve the problem would increase drastically.

The numerical implementation of the stress factor $\Delta\mathbf{q}$ has been done on integration point level (while calculating $\Delta\sigma$) and not on the global level of the internal forces ($\int_V \underline{B}^{T}\,\Delta \underset{\sim}{q}\,dV$ in (2.3.4)). The iterative Newton-Raphson scheme used to solve the global system of equations automatically corrects this error, and all equations are fully respected.

The time-step must be chosen such that the solution is sufficiently accurate. In addition of the requirements imposed by the stability of the integration scheme, one should assure a dynamically accurate solution. A critical time step size (Hughes, 1987) to impose is $\Delta t \le \frac{l_e}{c_l}$ where l_e is the element length and c_l is the longitudinal elastic wave velocity ($c_l = \sqrt{\frac{E}{\rho}}$).

A consistent mass matrix is used to reflect the mass distribution in the elements. In combination with an implicit scheme, this choice leads to more accurate results. All dynamic calculations have been performed with a time-integration parameter = 0.5 and Newmark parameters α = 0.5 and β = 0.25 (trapezoidal rule). This choice makes the Newmark method unconditionally stable ($\alpha \ge \frac{1}{2}$ and $\beta \ge \frac{(\alpha+\frac{1}{2})^2}{4}$)

This analysis will not deal with geometrical non linearity. Some results reflect strains that are to elevated to be modelled without a geometrical non-linear model. Nevertheless, the results are exploited, because the principal aim of this analysis is to verify the stabilising influence of the viscous contributions in the constitutive equations and not the exact calculation of the strains during deformation.

3. Numerical analyses

3.1. 2D-Tension Model

3.1.1. Wave propagation problem

3.1.1.1. Tension bar - Meshes

Numerical experiences are performed on the tension bar presented in fig 3.1.1. For reasons of symmetry only a fourth of the bar will be modelled by a finite element mesh.

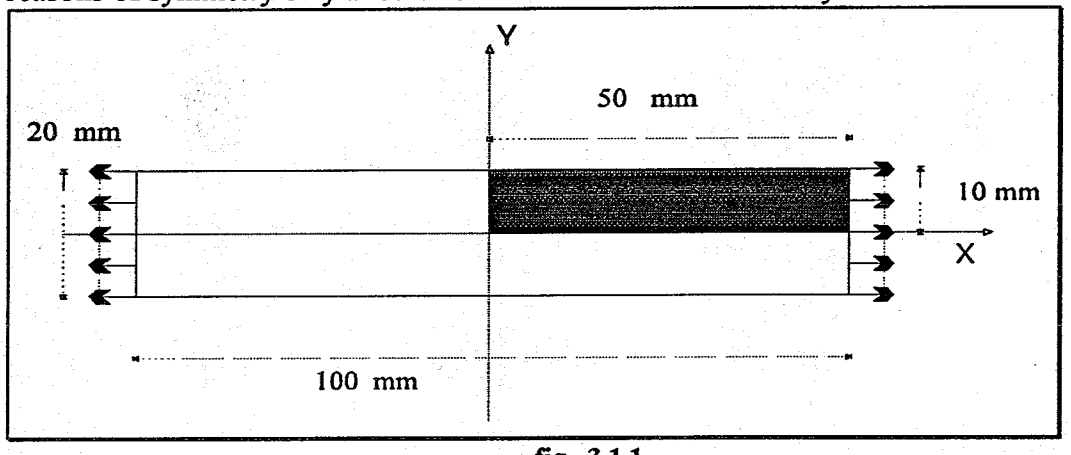

fig. 3.1.1

Mesh refinement is concentrated near the vertical symmetry-axis (Y-axis) from 2, 4, 8 to 16 elements over a range of 10 mm.

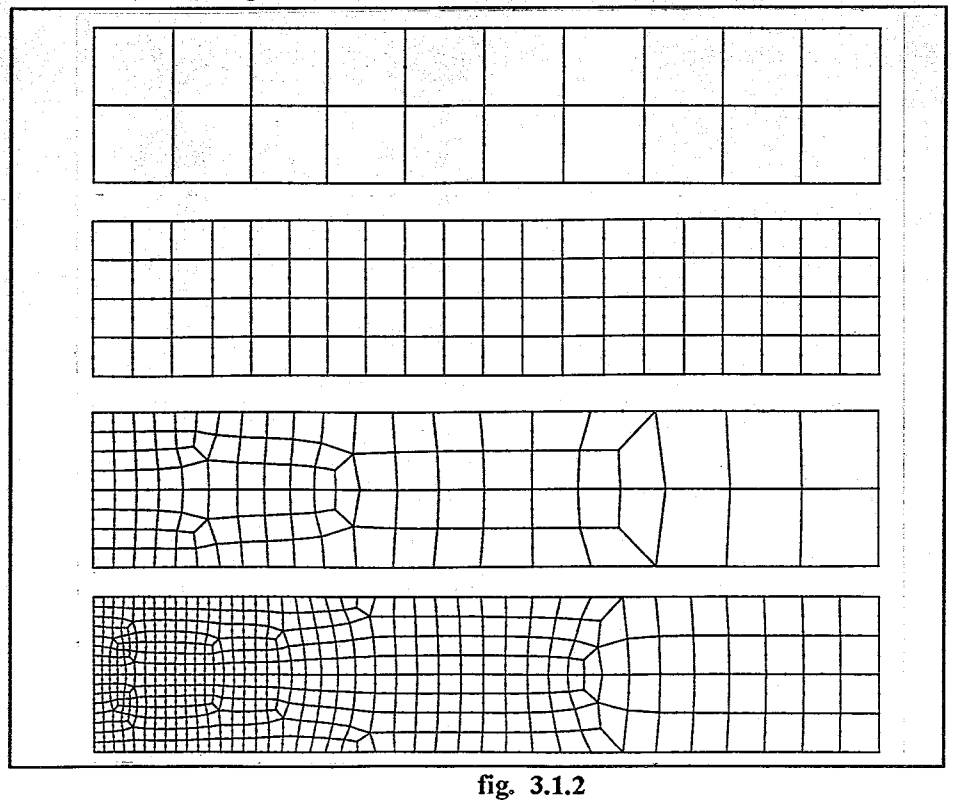

fig. 3.1.2

Symmetry-boundary conditions are applied on the symmetry-axes. The four meshes, used to examine localisation by wave-reflection, are visualised in fig 3.1.2. Use has been made of quadrilateral parabolic eight-noded isoparametric elements with a nine point Gauss integration scheme.

3.1.1.2. Geometry- & material parameters

Length mesh	=	50	mm
Width mesh	=	10	mm
Thickness	=	0.25	mm
Young's modulus	=	2000	MPa
Poisson's ratio	=	0.4	
Density	=	1000	$\frac{kg}{m^3}$

3.1.1.3. Boundary conditions - loading

Along the symmetry-axes, all displacement-components perpendicular to the axis are suppressed while all other components remain free. At the right boundary several loading-types were tested. It appeared that applying an increasing displacement (with a constant rate) results in a spurious solution as shown in figure 3.1.3 (load-displacement curve at the right edge). Although this solution seems to be unacceptable, mesh refinement leads to exactly the same curve. The inclusion of an algorithmic damping in time, to exclude artificial higher-order frequencies, or any variation of the time step (even for very small time-steps) still leads to the same solution. The results are probably due to the interaction of the incremental iterative integration on the one hand, and the rapid inertia-waves on the other hand. Numerically, the material cannot follow the imposed load rate. Other authors have also encountered similar problems.

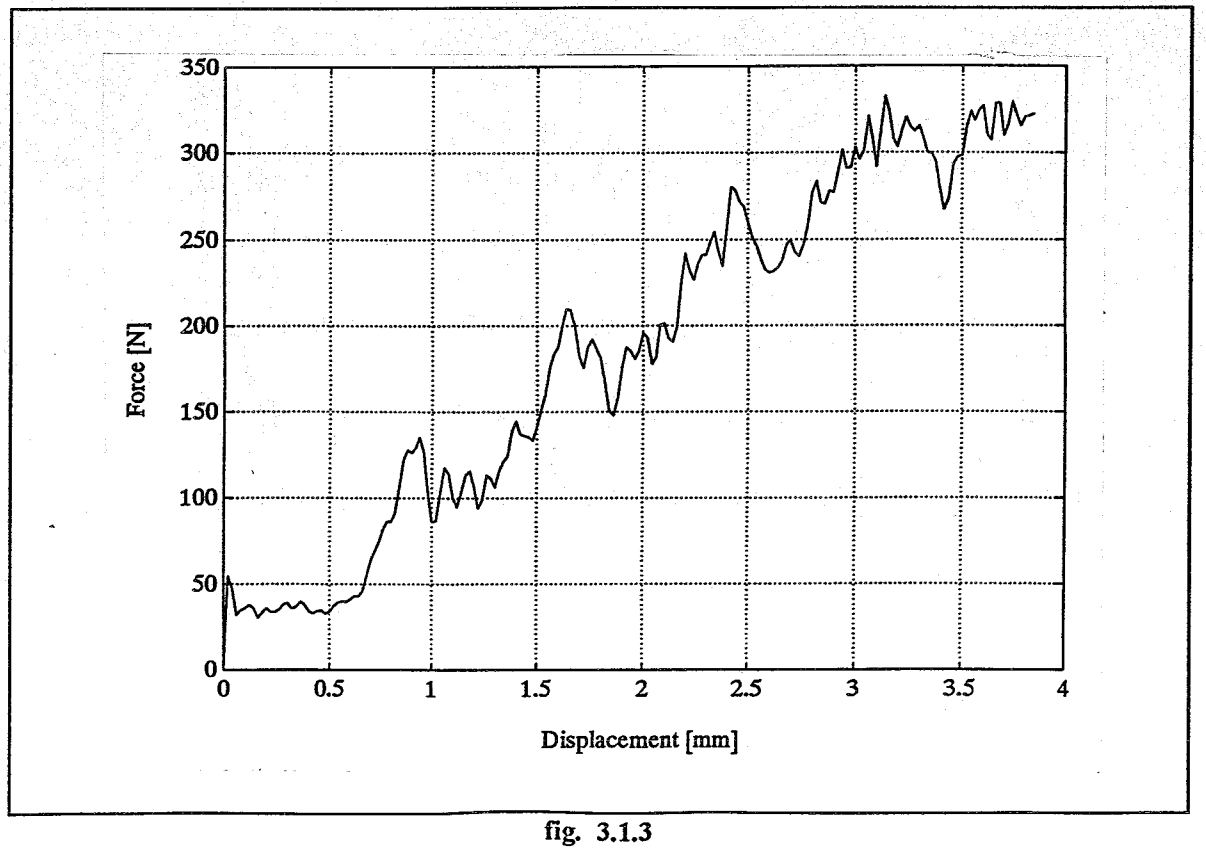

fig. 3.1.3

Another loading-type is used to exploit the results more efficiently. A block wave with a vertical stress front (fig. 3.1.3.b.) is applied to the right edge of the mesh (a fourth of the bar : fig 3.1.1.). The wave is applied by means of a uniformly distributed force. The load level has been chosen such that the response of the bar remains elastic until the left boundary is reached. The double in stress due to reflection of the tensile wave causes the triggering of localisation. The tensile wave propagates to the right and failure occurs before it reaches the right edge again.

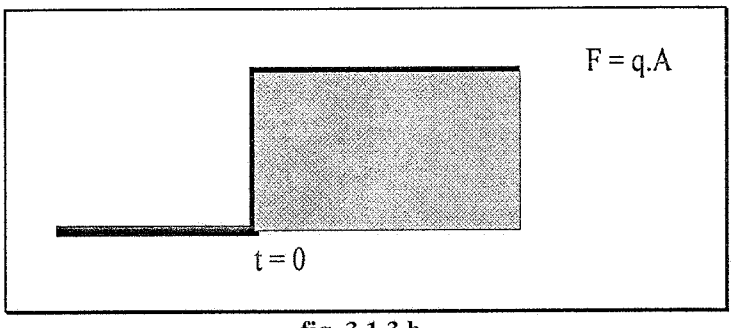

fig. 3.1.3.b.

The stress level **q** applied to the right edge is 11 MPa.

3.1.1.4. Viscous damage model

Model parameters

The following numerical values were used to simulate localisation throughout the viscous damage model.

Damage : $K = 1$ MPa/s^{-4}
$C = 15$ s^{-1}
$r = 4$
$D_c = 0.8$

Damage initiation starts at a stress-level $\bar{\sigma}_o$ equal to 15 MPa, which is exceeded after reflection.

The time step used for the time-integration is chosen mesh-dependent at ± 50 % of the critical time-step (calculated with the smallest element). This choice is justified in §2.3.3.

Coarse Mesh : $\Delta t = 16.10^{-7}$ s

Medium Mesh : $\Delta t = 8.10^{-7}$ s

Fine Mesh : $\Delta t = 4.10^{-7}$ s

Extra fine Mesh : $\Delta t = 2.10^{-7}$ s

The elastic wave speed obtained with the numeric values of §3.1.1.2. is 1414 m/s.

Results

The results of the axial strains along the symmetry-axis of the bar (X-axis) is shown in fig 3.1.4. The localisation stabilises and the fine meshes globally present the same localisation width. All results have been taken at time 64 μs, which corresponds with load step 40, 80, 160 and 320 respectively for each mesh. At 64 μs, the loading wave traversed 90 mm (50 mm elastically, 40 mm after reflection). At this time failure occurs because the critical damage is reached in a small zone of the bar. The coarse mesh is somehow a little to scabrous and cannot really represent the fine localisation zone. Fig 3.1.5 represents the same results at an earlier stage (time 50 μs), where the wave traversed 70 mm.

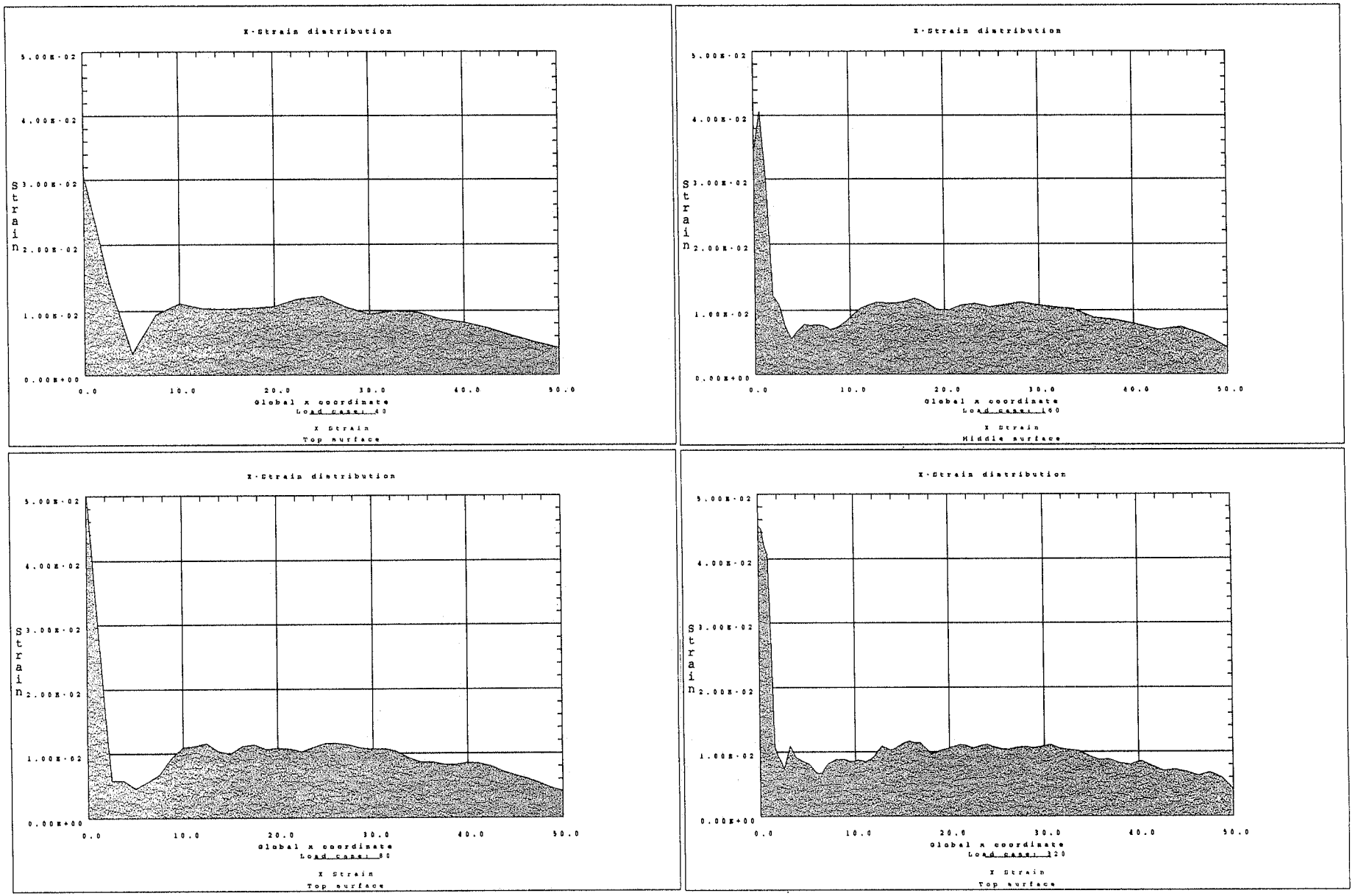

Fig 3.1.4. **Axial strains on symmetry-axis at 64 μs - 2D-Tension model - viscous damage model : Coarse mesh (upper left corner) , Medium mesh (lower left corner), Fine mesh (upper right corner), Extra fine mesh (lower right corner)**

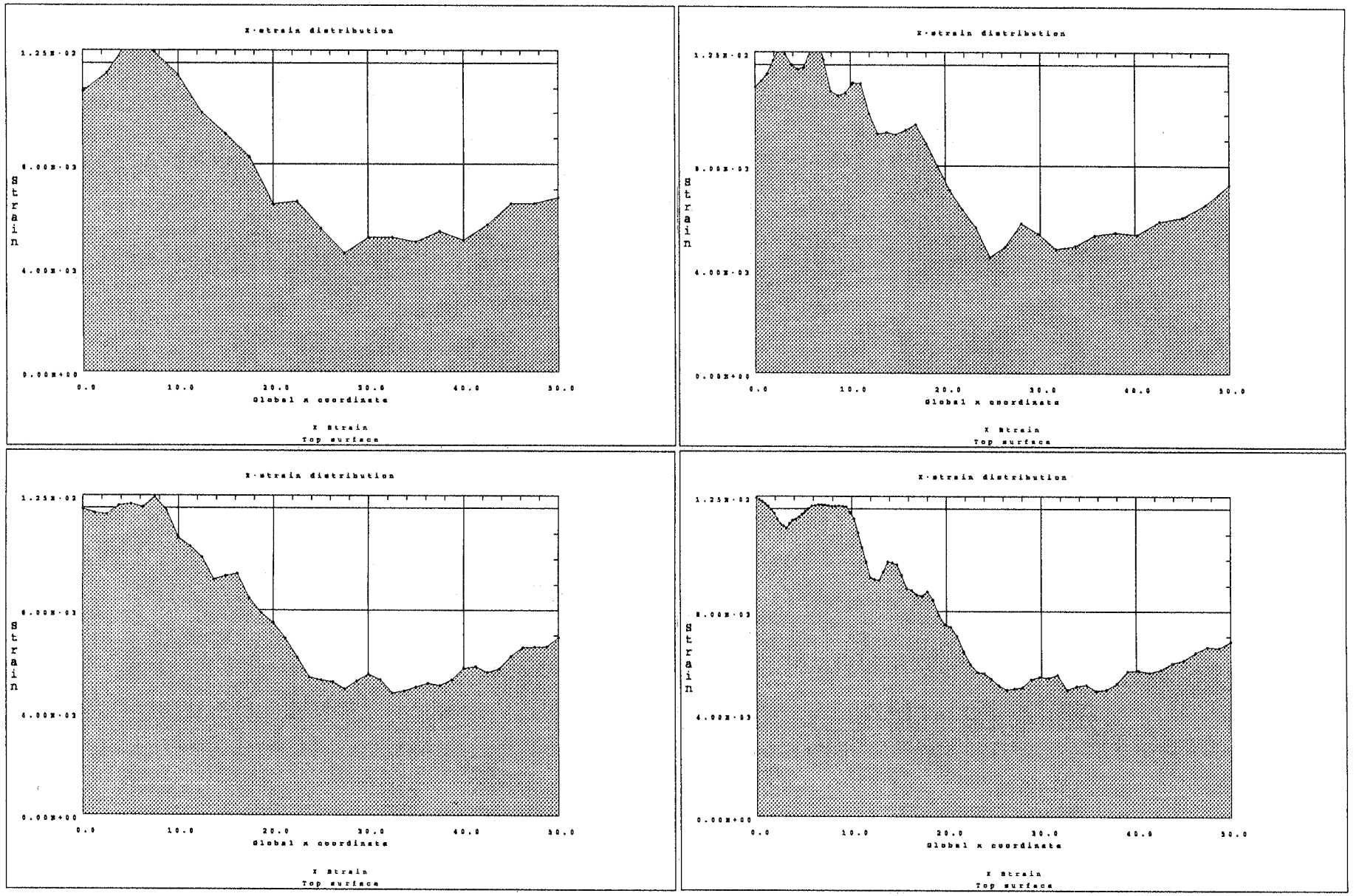

Fig 3.1.5. **Axial strains on symmetry-axis at 50 μs - 2D-Tension model - viscous damage model : Coarse mesh (upper left corner) , Medium mesh (lower left corner), Fine mesh (upper right corner), Extra fine mesh (lower right corner)**

Strains are smaller and the global localisation zone is still wider, but mesh objectivity remains globally preserved. The strain-development that nicely reflects the wave propagation and the appearance of the localisation zone is represented in fig. 3.1.6 below. Reflection occurred at time step (time 35 μs).. The deformed mesh in the failure stage is given in figure 3.1.7 below.

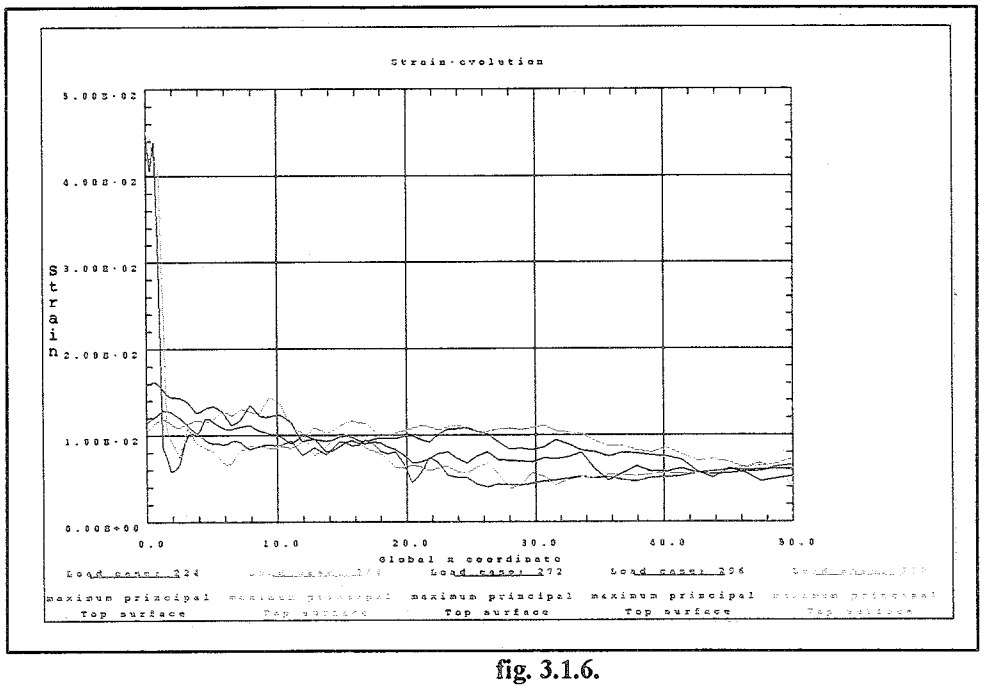

fig. 3.1.6.

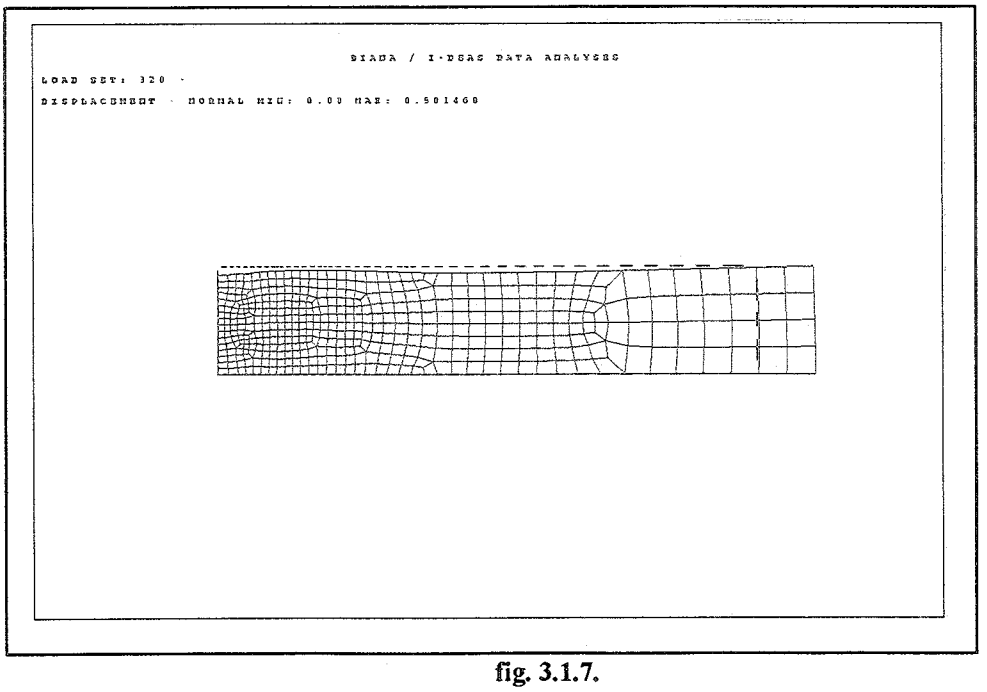

fig. 3.1.7.

It is also interesting to analyse the local strain distribution in the bar, which shows more 2D-effects. Fig. 3.1.8. and fig 3.1.9 show the results for the four meshes. Again, the coarse mesh is represented in the upper left corner, the medium mesh in the lower left corner, the fine mesh in the upper right corner and the extra fine mesh in the lower right

corner. Fig 3.1.8 was taken at time 64 μs and fig 3.1.9 at time 50 μs. Locally some small differences occur on fig. 3.1.8.. On the local level, mesh orientation slightly influences the results in the final stage of the failure mechanism, when damage increases rapidly. This rapid increase of damage and strain is precisely the cause of the local numeric differences that appear between the meshes. These differences are very small in fig 3.1.9, where damage has not yet attained a high value.

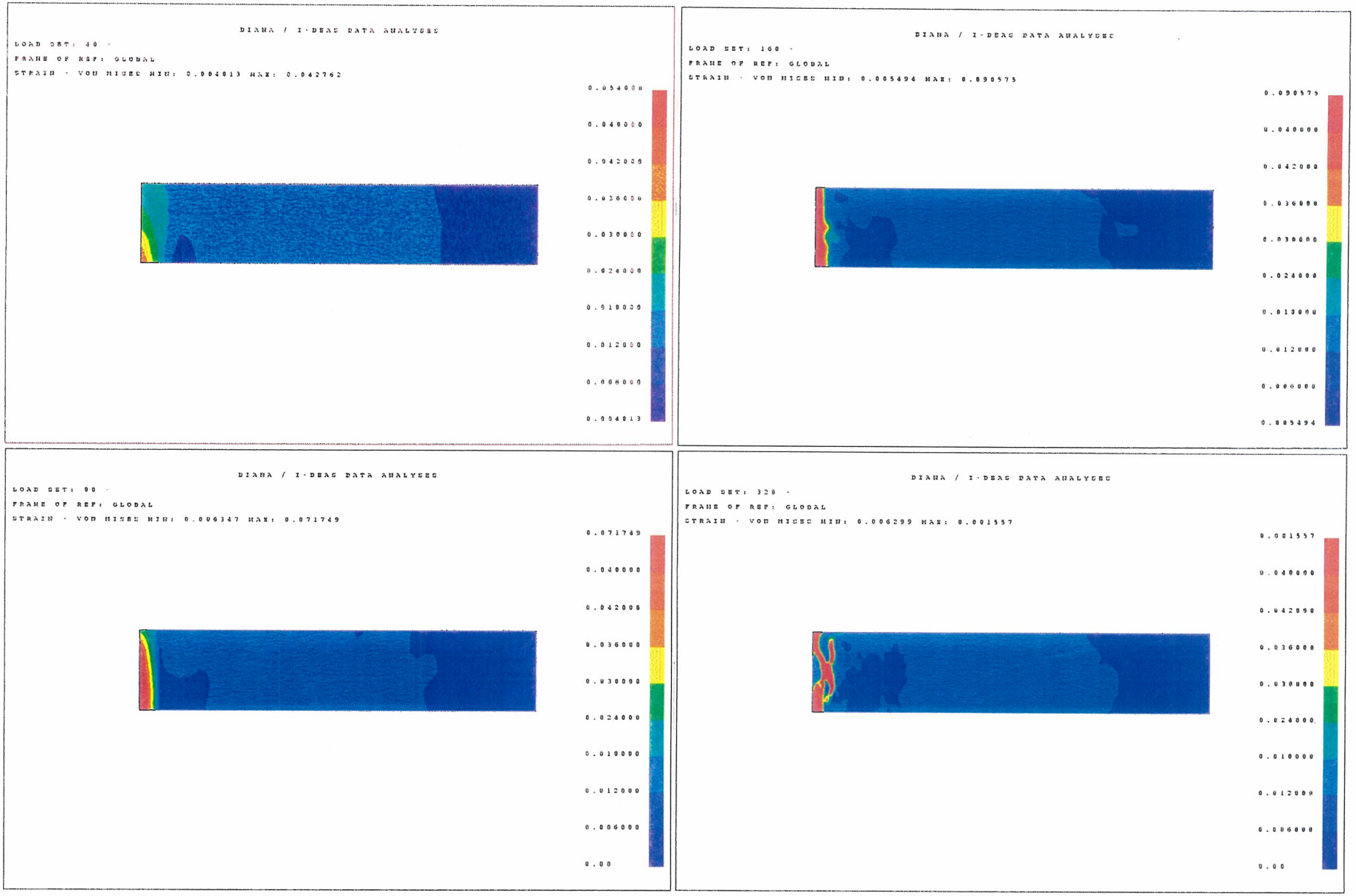

Fig 3.1.8. **Von Mises strains at 64 μs - 2D-Tension model - viscous damage model : Coarse mesh (upper left corner) , Medium mesh (lower left corner), Fine mesh (upper right corner), Extra fine mesh (lower right corner)**

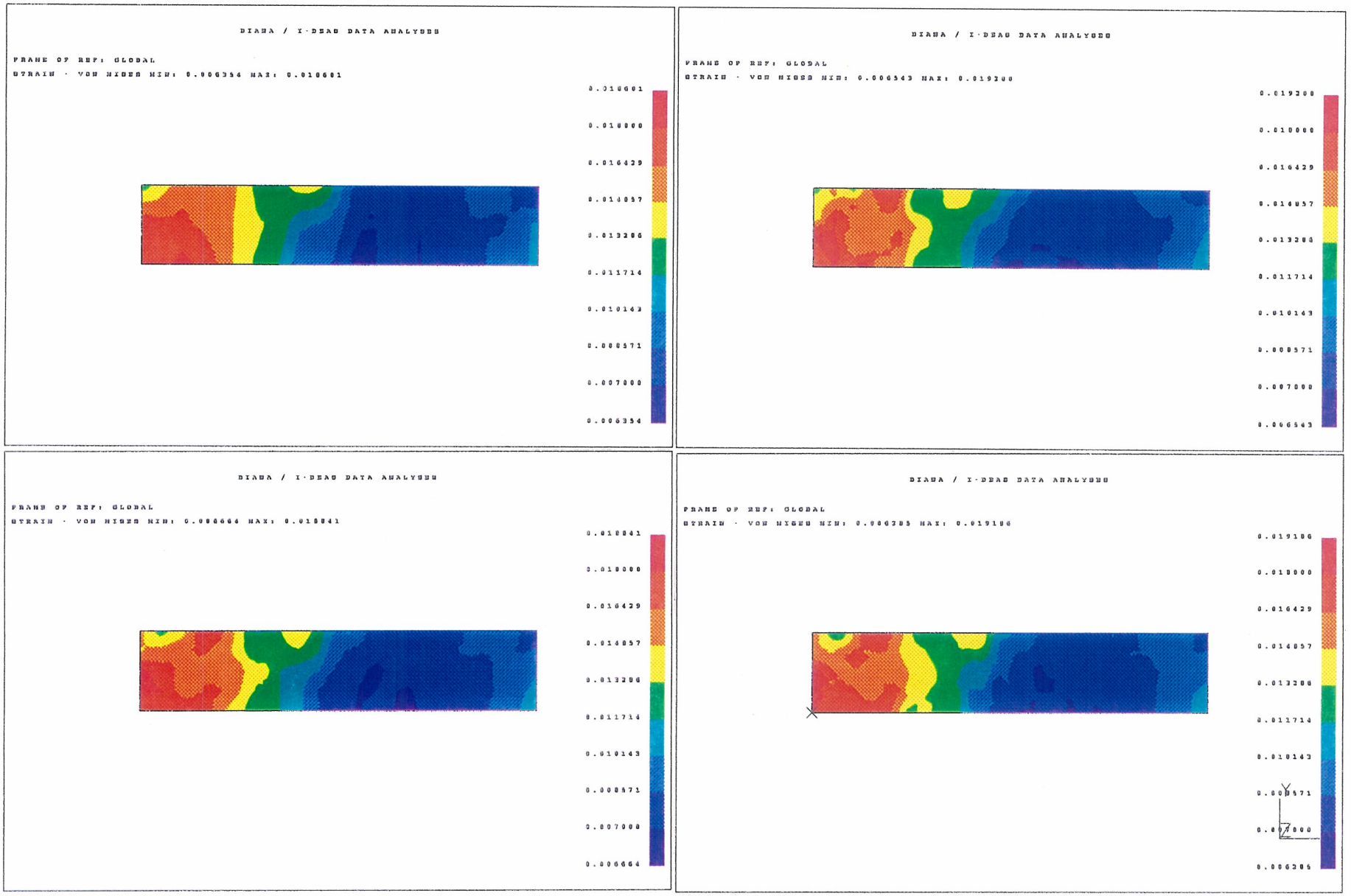

Fig 3.1.9. **Von Mises strains at 50 μs - 2D-Tension model - viscous damage model : Coarse mesh (upper left corner) , Medium mesh (lower left corner), Fine mesh (upper right corner), Extra fine mesh (lower right corner)**

3.1.1.5.Perzyna's viscoplastic model involving damage

Model parameters

Following numerical values were used to simulate localisation by the viscoplastic damage-model.

Damage : $K = 0{,}3\ MPa/s^{-3}$
$C = 50\ s^{-1}$
$r = 3$
$D_c = 0.8$ D_c stands for the critical damage level (= the maximum achievable damage)

Viscoplasticity : $\gamma = 100\ s^{-1}$
$N = 2$
$\kappa = 15\ MPa$

The yield limit κ and the damage threshold K.C are fixed at 15 MPa. The time-step is chosen identically to the value in §3.1.1.4.

The exponent in the damage evolution law is taken smaller than in the previous paragraph. The exponential character of the damage evolution law is decreased in favour of the viscosity of Perzyna's model. The value 100 s^{-1} for γ is necessary to permit the rise of the viscoplastic strain in a short time.

Results

The results are taken at the same instants as in the viscous damage model. Fig 3.1.10. shows a typical deformed mesh. Fig 3.1.11 presents the axial strains along the symmetry-axis for the four meshes.

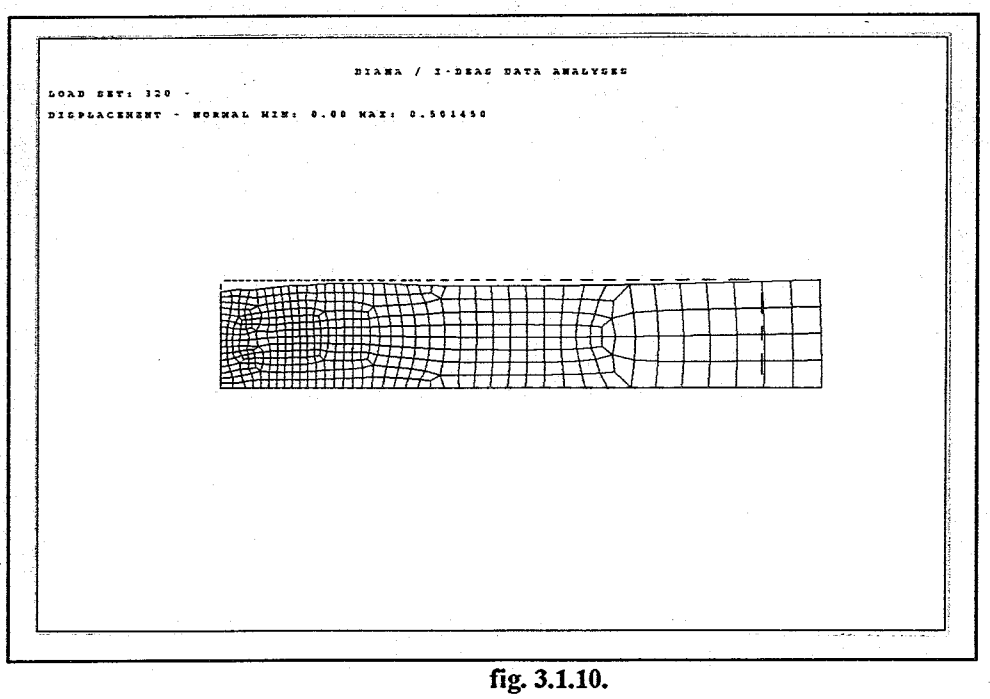

fig. 3.1.10.

It can be observed that the stress distribution in the bar is smoother with the viscoplastic model. This twofold model is more capable to fit to different strain-patterns that can be measured by experiments. The damage ensures the localisation, while the global double viscosity takes care of the regularization. The 2D-plots of the Von Mises strains in fig. 3.1.12. on page 23, show that some small differences remain between the meshes in the failure stage.

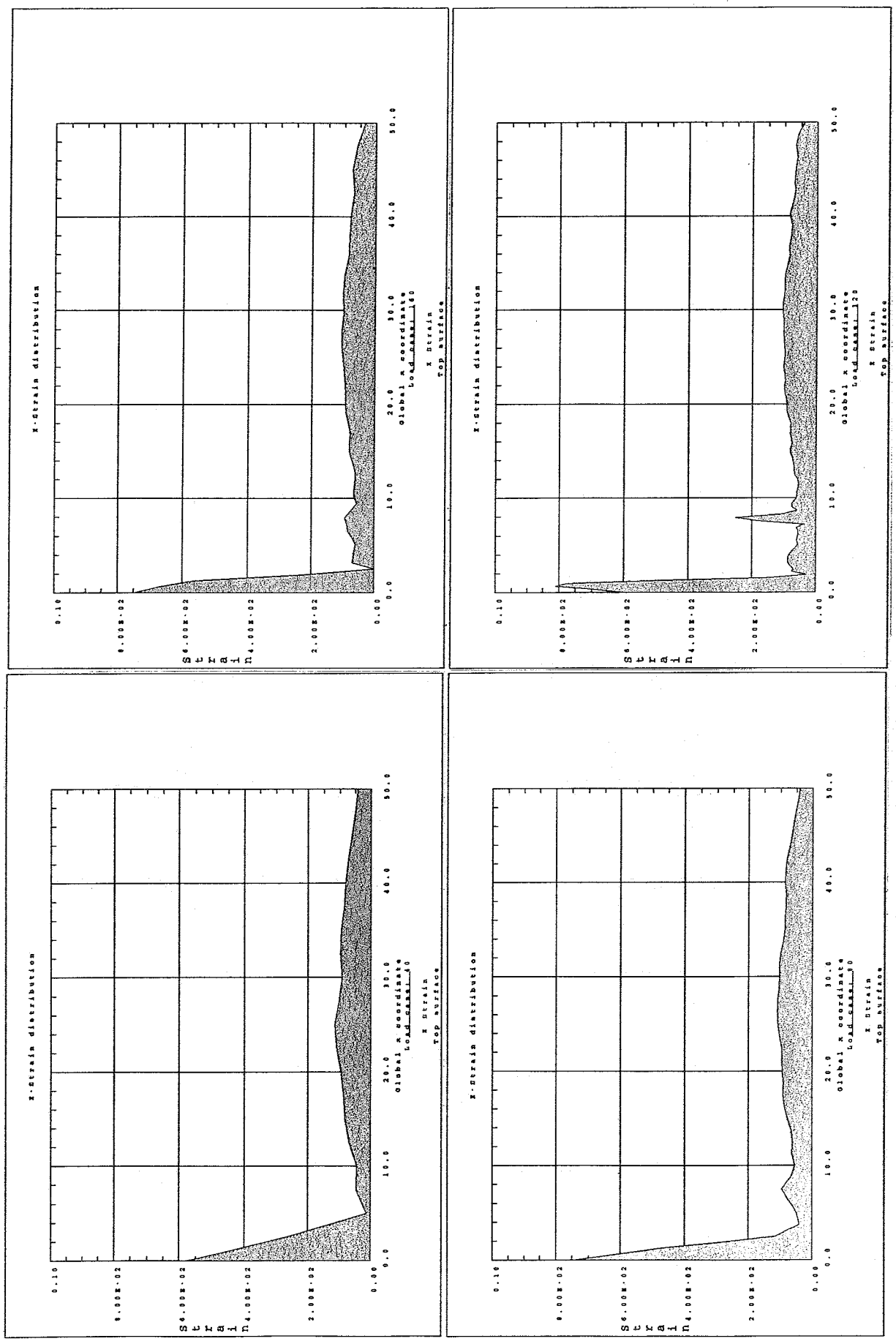

Fig 3.1.11. Axial strains on symmetry-axis at 64 μs - 2D-Tension model - Perzyna's viscoplasticity involving damage : Coarse mesh (upper left corner), Medium mesh (lower left corner), Fine mesh (upper right corner), Extra fine mesh (lower right corner)

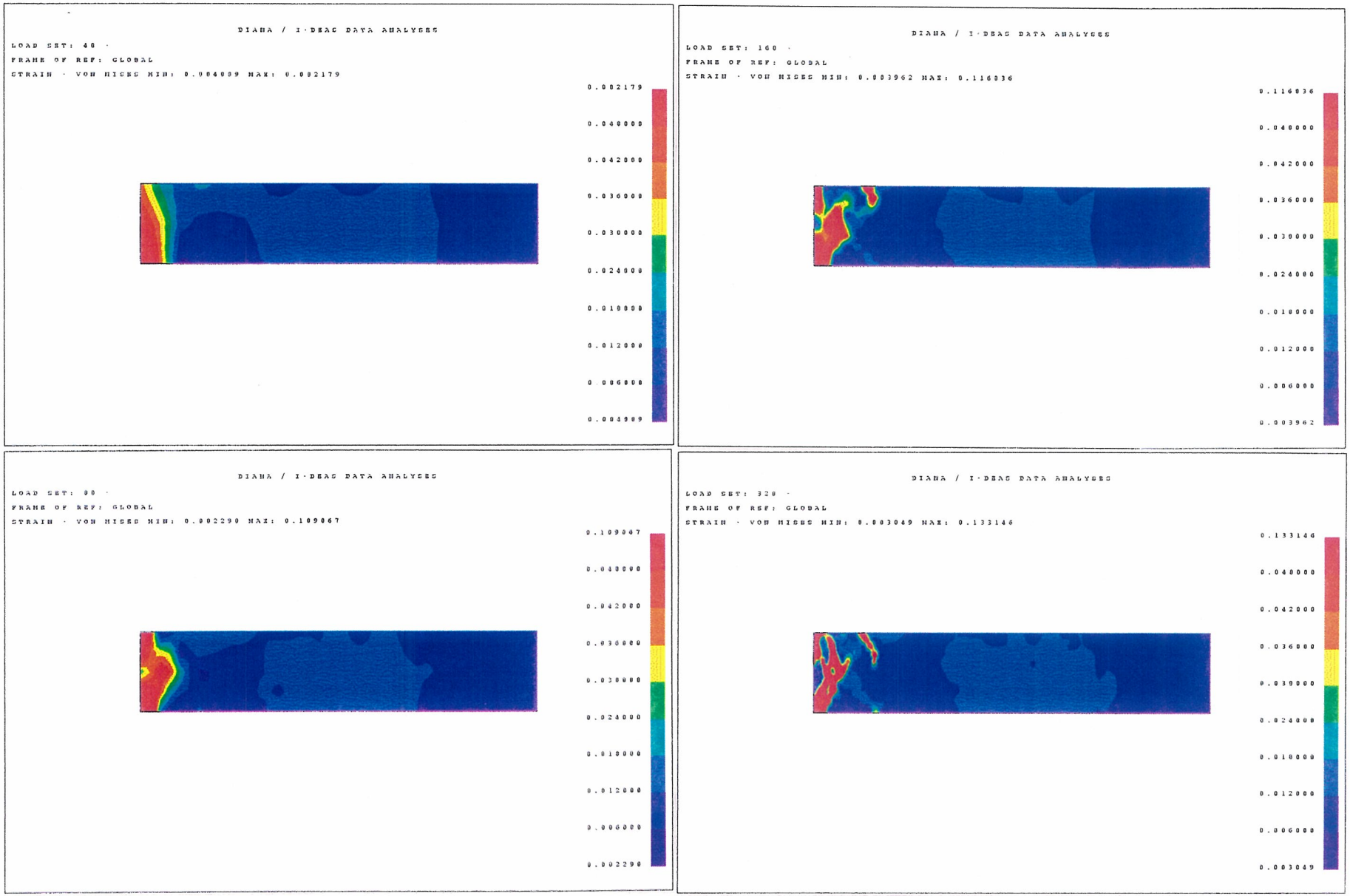

Fig 3.1.12. **Von Mises strains at 64 μs - 2D-Tension model - Perzyna's viscoplasticity involving damage : Coarse mesh (upper left corner) , Medium mesh (lower left corner), Fine mesh (upper right corner), Extra fine mesh (lower right corner)**

3.1.2. Viscous analysis without inertia-effects

3.1.2.1. Tension bar - Meshes

Without inertia effects, the load is immediately transferred to the whole bar. The load level must exceed the yield limit or the damage limit to get strain-softening. Some kind of imperfection must be used to trigger localisation in a certain point or area. Many possibilities are available to create a *weaker* zone in the bar, from where localisation starts. In this study six different type of imperfections were used to overcome this problem.

1. Reduction of the element thickness
2. Applying a supplementary small load
3. Applying a supplementary small displacement
4. Using a small initial damage in some integration points
5. Using a tension bar with a conical varying section
6. Using a tension bar with a circular varying section

A commonly used type is the reduction of thickness of certain elements. It was found that such an imperfection favourites the localisation in a zone that depends on the width of the adapted elements. The size of the reduction also influences the localisation-time and the final results. Applying supplementary loads or displacements leads to results that are strongly dependent on the load-type. Another promising imperfection is the use of initial damage in some integration points (near the vertical symmetry-axis). The localisation that can be obtained is very clear. Nevertheless this imperfection is not used for further analysis because it induces an inherent mesh-dependence. The initial damage values on integration point level are numerically treated continuously during integration on element-level. Consequently, the width of the weakened zone that corresponds with an integration point depends on the size of the mesh.

Finally an imperfection of the geometry is used. The tension bar of fig 3.1.1 is modified by reducing the width at the centre of the bar from 20 mm to 19 mm. A linear variation (conical bar) between 20 mm at the right edge and 19 mm in the centre, leads to a localisation pattern that starts from the angular point on the Y-axis. To avoid this a quadratic variation is used (which leads to a circular-type) with the centre of curvature on the Y-axis. The three meshes that are built on this last model are visualised in fig 3.1.13.

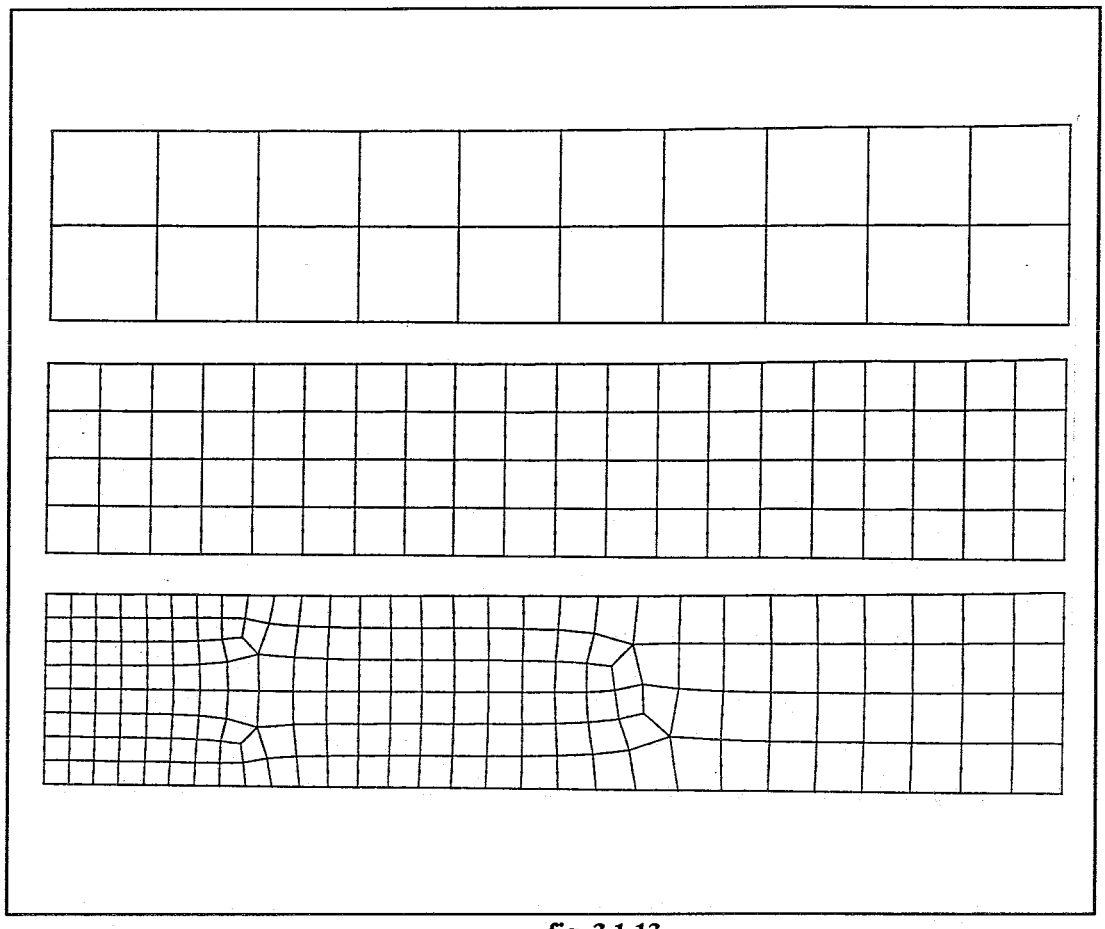

fig. 3.1.13

Symmetry-boundary conditions are applied on the left and lower boundary of the mesh. Quadrilateral parabolic eight-noded isoparametric elements with a nine-point Gauss-integration scheme are used.
The material parameters are identical to those of §3.1.1.2.

3.1.2.2. Boundary conditions - loading

A comparison with the dynamic model is not very useful. In the dynamic model the load-level was kept under the yield limit to trigger localisation after wave-reflection. In this case the load-level must exceed the yield-limit. A block wave cannot be used reasonably when there is no wave propagation. Therefore a linear time-varying displacement (constant rate) was used to excite the model. The numerical tests were performed with two different load-rates, 0.01 mm/s and 0,1 mm/s.

3.1.2.3. Viscoplastic damage-model

Model parameters

Damage : $K = 15$ MPa/s^{-3}
$C = 1$ s^{-1}
$r = 3$
$D_c = 0.8$

Viscoplasticity : $\gamma = 0.02$ s^{-1}

$N = 3$

$\kappa = 15$ MPa

The time-domain of this analysis is fundamentally different from the one used in the dynamic analysis. The numerical values of the damage parameters and the viscosity in Perzyna's model are chosen differently. The yield limit is approximately exceeded after a displacement of 0.38 mm, or 38 s for the slow rate and 3.8 s for the medium rate. The elastic part of the loading is calculated with a large time-step, while a smaller time step is used for the remaining viscoplastic-softening part. For all three meshes 0,25 s (slow rate) and 0,025 s (medium rate) are used as time-steps. The integration parameter θ is taken equal to 0,5.

Results - slow rate load

All results are taken at time . The deformed fine mesh is represented in fig 3.1.14. Fig 3.1.15 shows the comparison between the different meshes. The axial strain evolution (in time) on the symmetry-axis is represented in figure 3.1.16 for the fine mesh. All results are taken at time 57,5 s which corresponds with load step 97 and a global displacement of 0,575 mm at the right edge.

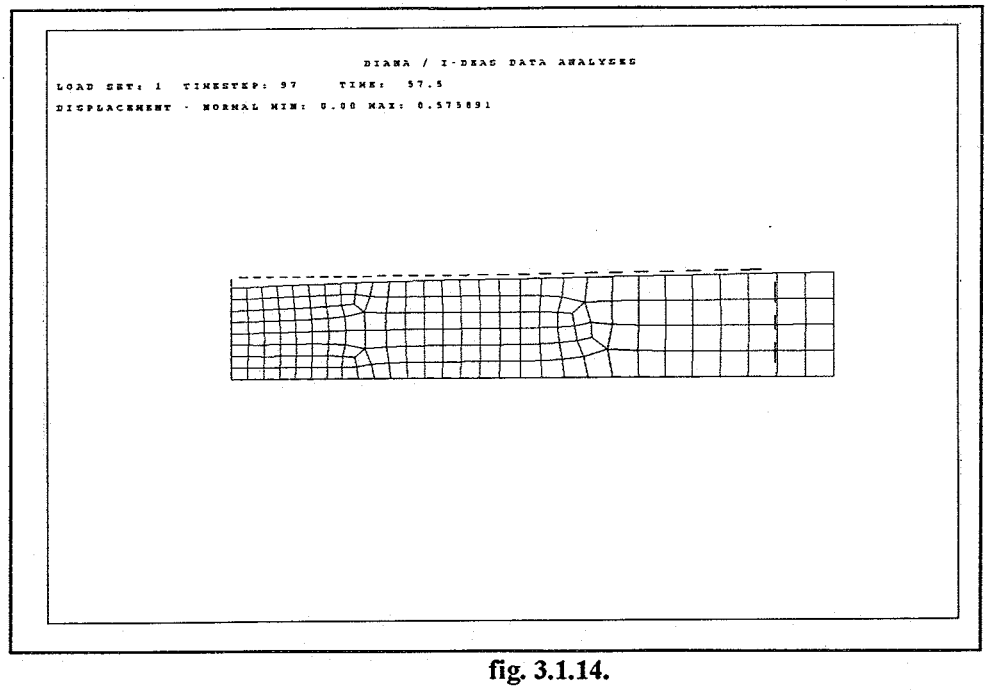

fig. 3.1.14.

Globally, mesh-objectivity is still preserved for the applied load-rate. The viscosity γ and the damage parameters K and C must be well chosen for a certain range of load-rates. For this example, other values were used where mesh-sensitivity clearly appeared. Slow rates need a small value for γ. On the other hand, if γ becomes to small, the failure mechanism will be entirely controlled by damage. The parameters of the damage evolution law of Perzyna's viscoplastic model must be fitted to one another to obtain acceptable mesh-insensitive results. This complicates an adequate choice of a parameter-set to describe a material's behaviour correctly. Figure 3.1.17 shows the Von Mises strains that are calculated with the fine mesh. Again, it is obvious that 2D-effects (little shear bands) appear in the final failure stage.

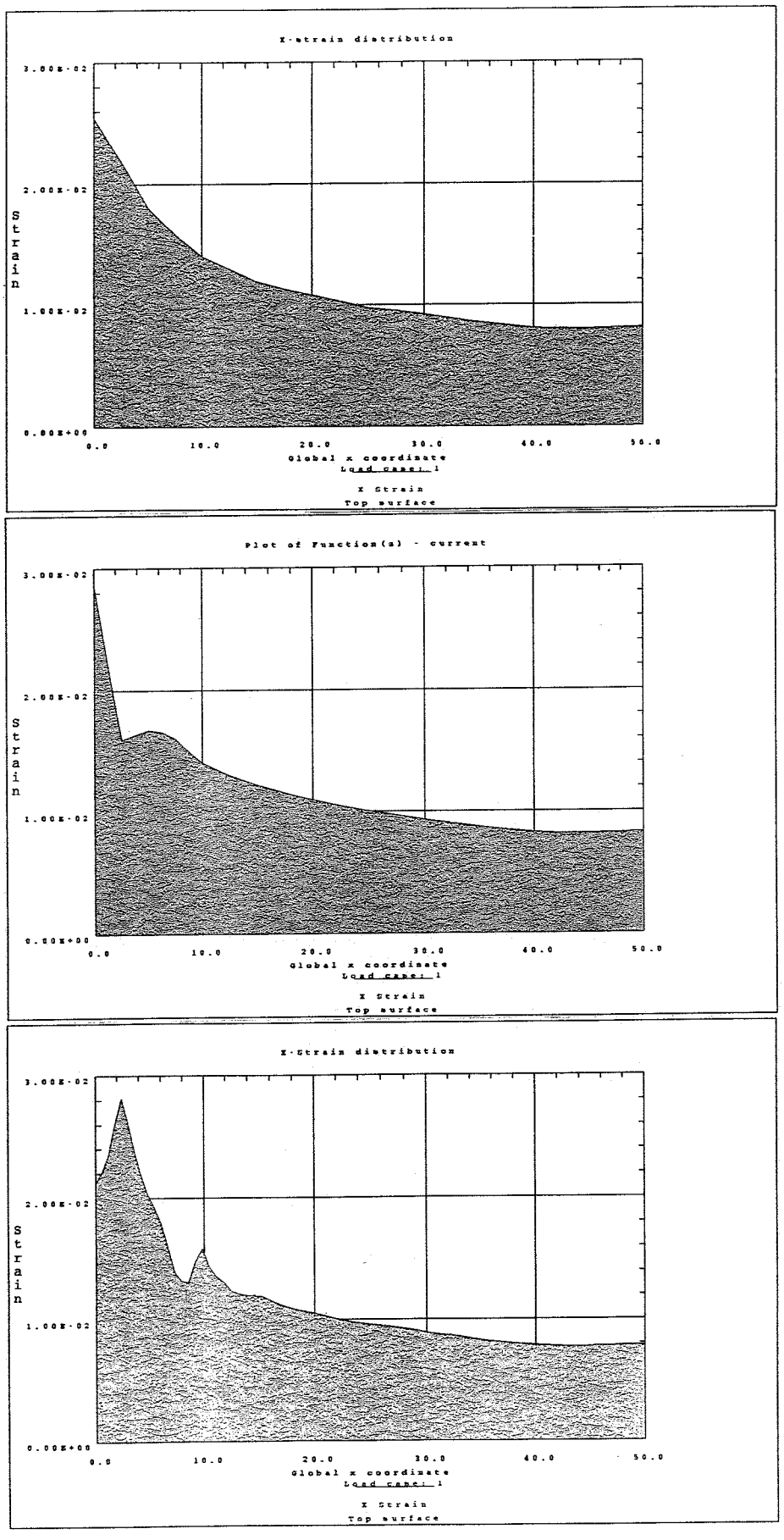

Fig 3.1.15. Axial strains on symmetry-axis at 57,5 s - 2D-Tension model, slow load rate - Perzyna's viscoplastic model involving damage : Coarse mesh (top), Medium mesh (centre), Fine mesh (bottom)

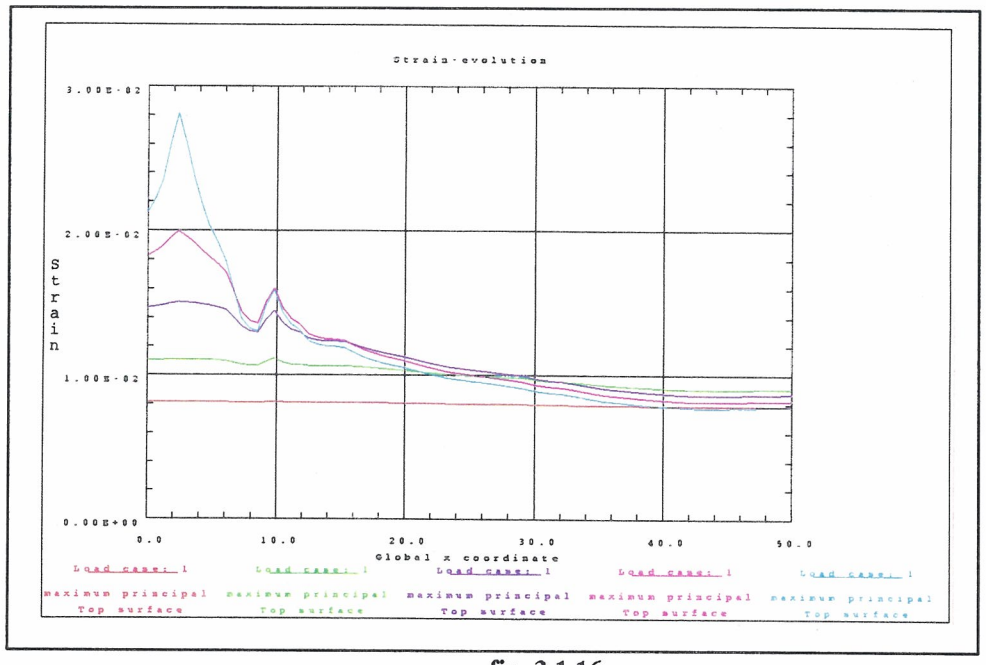

fig. 3.1.16.

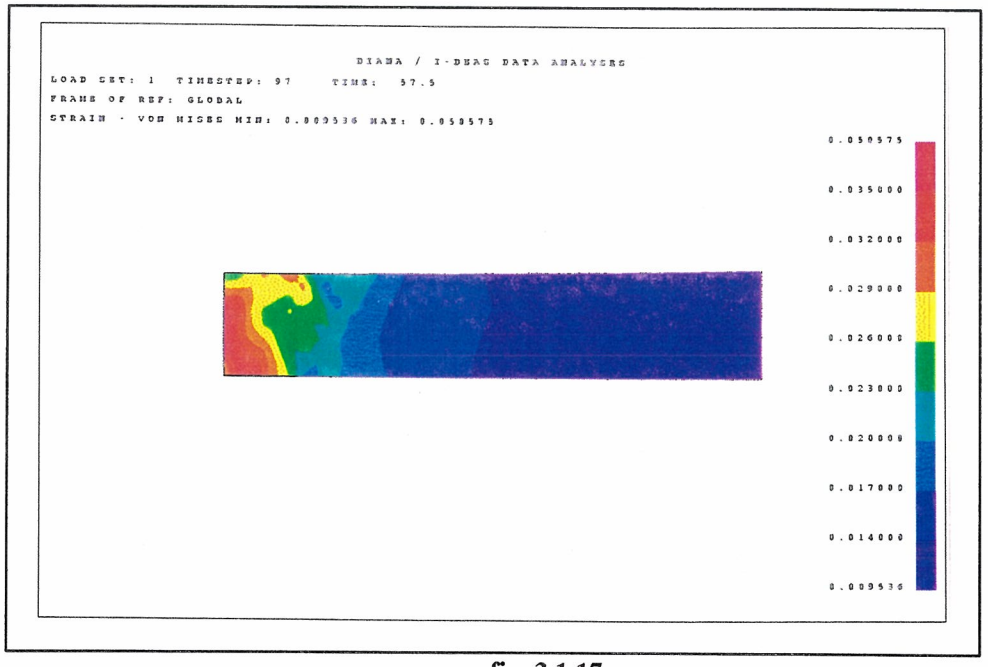

fig. 3.1.17.

Results medium rate load

To evaluate the influence of the load-rate and the viscous rate-dependence a second analysis is carried out on the same meshes. The results are taken at time 7,5 s (load step 127) before failure occurred. The imposed displacement is 0,075 mm at this time. Fig 3.1.18 represents the axial strains for the three meshes. This figure clearly shows the viscous character of the constitutive model. A larger global displacement leads to smaller strains in a wider localisation zone. Localisation is relatively delayed. Fig 3.1.19 represents the load-displacement curves for both rates with their global softening branches. The comparison between the three meshes is shown in fig. 3.1.20 for both rates. No differences can be observed, which confirms the global mesh-insensitivity.

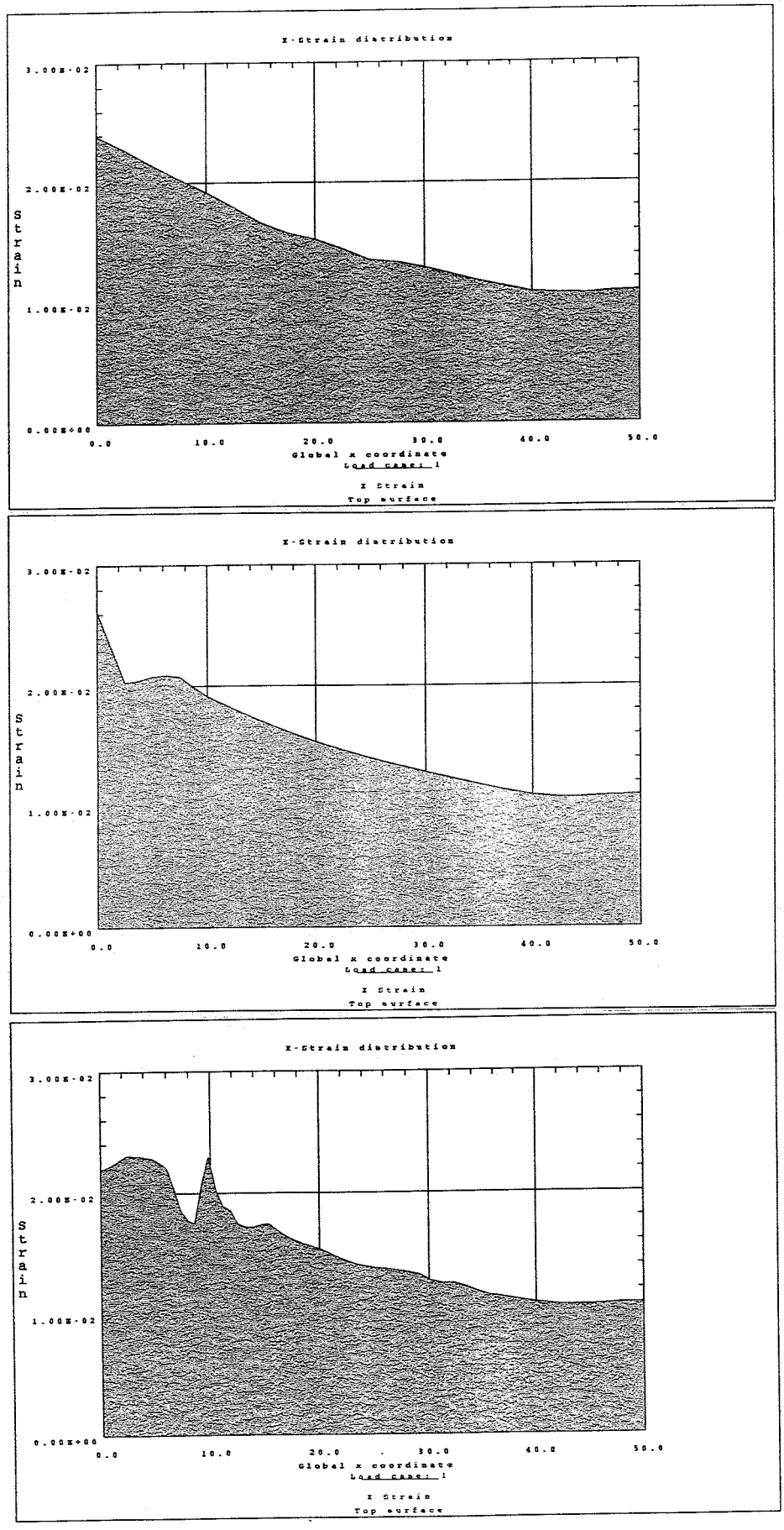

Fig 3.1.18. Axial strains on symmetry-axis at 7,5 s - 2D-Tension model, medium load rate - Perzyna's viscoplastic model involving damage : Coarse mesh (top), Medium mesh (centre), Fine mesh (bottom)

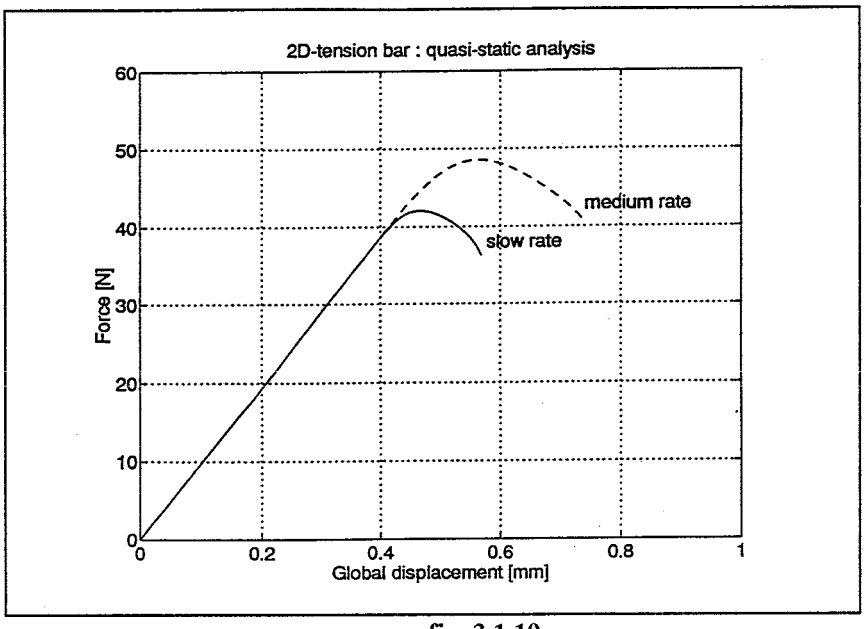

fig. 3.1.19.

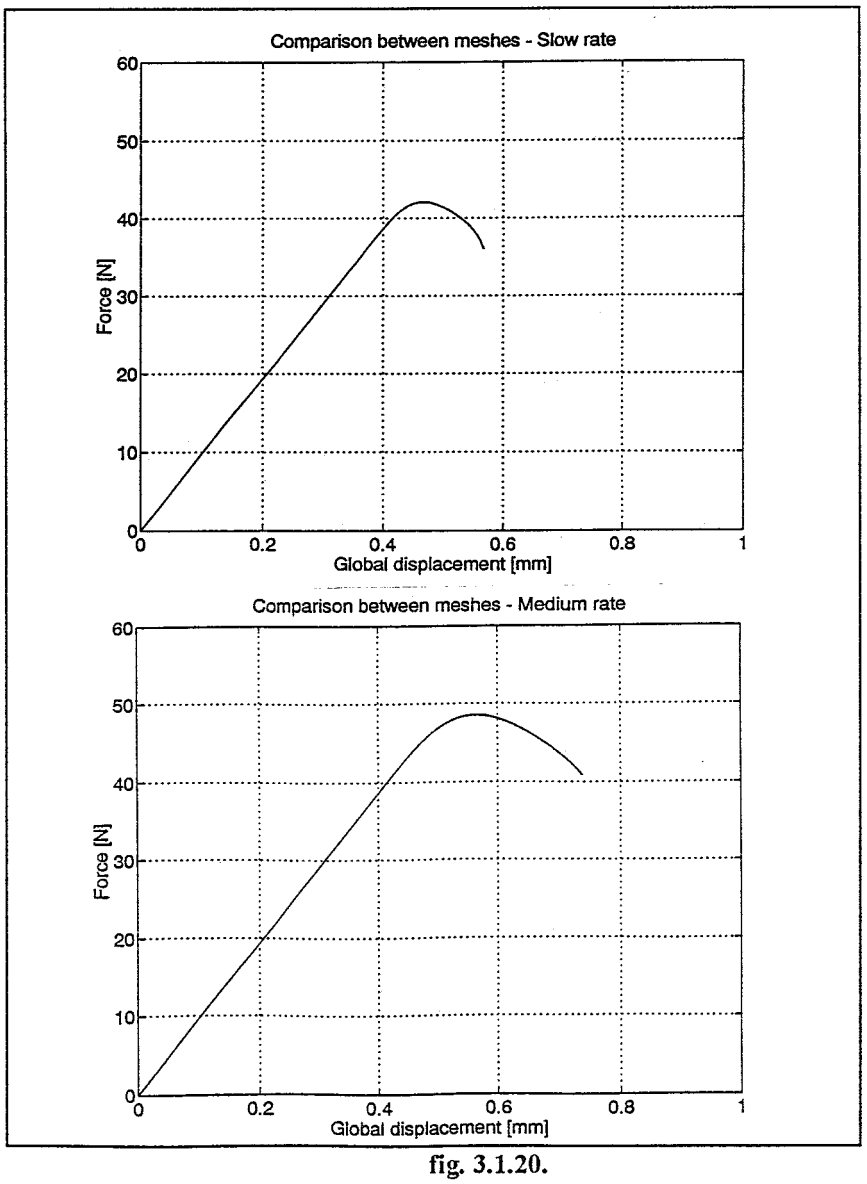

fig. 3.1.20.

3.2. Shear layer model

3.2.1. Model - meshes - boundary conditions - loading

A 1D-shear model is used to check and compare the results for a different material, with a different geometry and in mode II-localisation (Sluys 1992). The verification has been done for the dynamic analysis, including inertia-effects. The sketch of the model is given in fig 3.2.1. The layer can be taken from a semi-infinite strip.

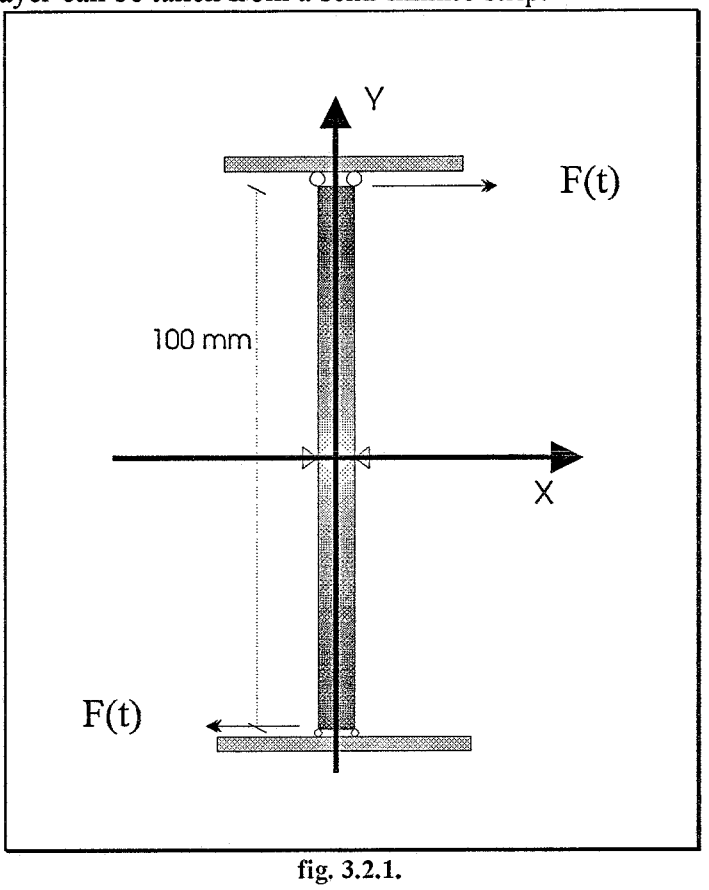

fig. 3.2.1.

On this model four meshes are build, with progressively refined elements. The width of the strip is refined with the mesh (the elements remain square). A plot of the four meshes is given in figure 3.2.2. Quadrilateral linear four-noded isoparametric elements with a nine point Gauss integration scheme are used. In the centre of the layer (X-axis) the horizontal displacements are restrained to zero because of symmetry considerations. All displacements in the y-direction are constrained to zero. Additional linear constraints need to be applied to render the problem one-dimensional. All horizontal displacements of the nodes on a same y-level are set equal to one another. A block wave is applied to the upper and lower boundary as sketched in figure 3.2.1.

Geometry and material parameters

Coarse mesh :	20 elements	5 mm x 5 mm	Layer width = 5 mm
Medium mesh :	40 elements	2,5 mm x 2,5 mm	Layer width = 2,5 mm
Fine mesh :	80 elements	1,25 mm x 1,25 mm	Layer width = 1,25 mm
Extra fine mesh :	160 elements	0,75 mm x 0,75 mm	Layer width = 0,75 mm

Thickness = 0,1 mm
Young's modulus E = 9800 MPa

Poisson's ratio $\nu = 0,4$
Density $\rho = 500\ kg/m^3$

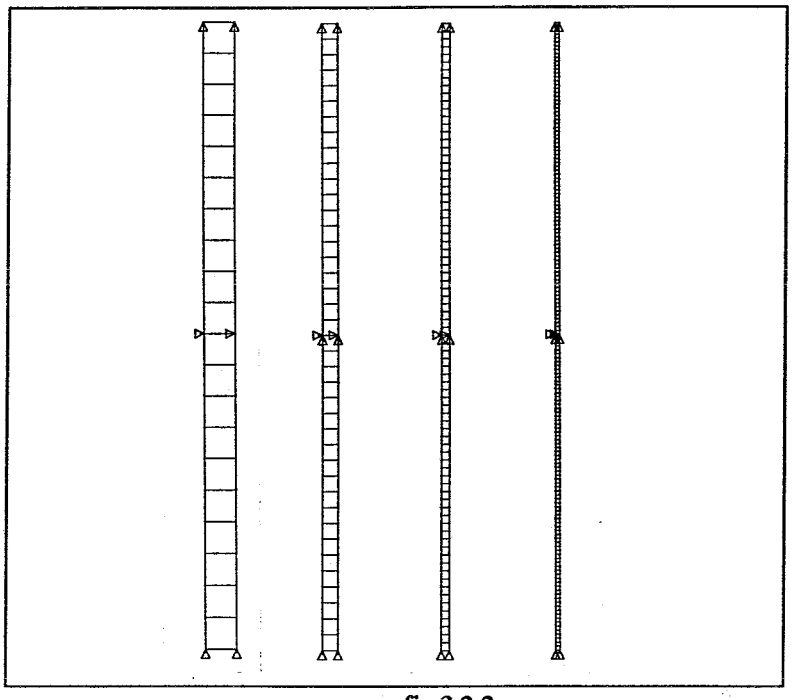

fig 3.2.2

The integration parameter θ is taken equal to 0,5. The shear wave velocity is given by $c_s = \sqrt{\frac{\mu}{\rho}}$ where μ stand for the shear modulus $\mu = \frac{E}{2(1+\nu)}$. For the chosen material a shear wave velocity of 2646 m/s is found. The two shear waves start from the upper and lower boundary, meet in the middle and reflect toward the boundaries again. The total time to cross over the length of the layer is approximately 38 μs. The time-step is chosen mesh-dependent for reasons of dynamic stability (§3.1.1.4 and 2.3.3).

Coarse mesh : $\Delta t = 10.10^{-7}$ s

Medium mesh : $\Delta t = 5.10^{-7}$ s

Fine mesh : $\Delta t = 25.10^{-8}$ s

Extra fine mesh : $\Delta t = 12,5.10^{-8}$ s

A block wave with a vertical stress front is applied to the upper and lower boundary, analogous to §3.1.1.3. The load **F** is taken equal to **q.A** where **q** stands for the shear stress load and **A** for the mesh-dependent cross-section area of the layer. The shear stress level is taken equal to 40% of the yield limit. After reflection in the centre of the layer the yield limit will be exceeded. The yield limit for the viscoplastic model and the damage threshold value are both fixed at 100 MPa.

3.2.2. Viscous damage regularization

Model parameters

Damage : $K = 2\ MPa/s^{-4}$
$C = 50\ s^{-1}$
$r = 4$
$D_c = 0.8$

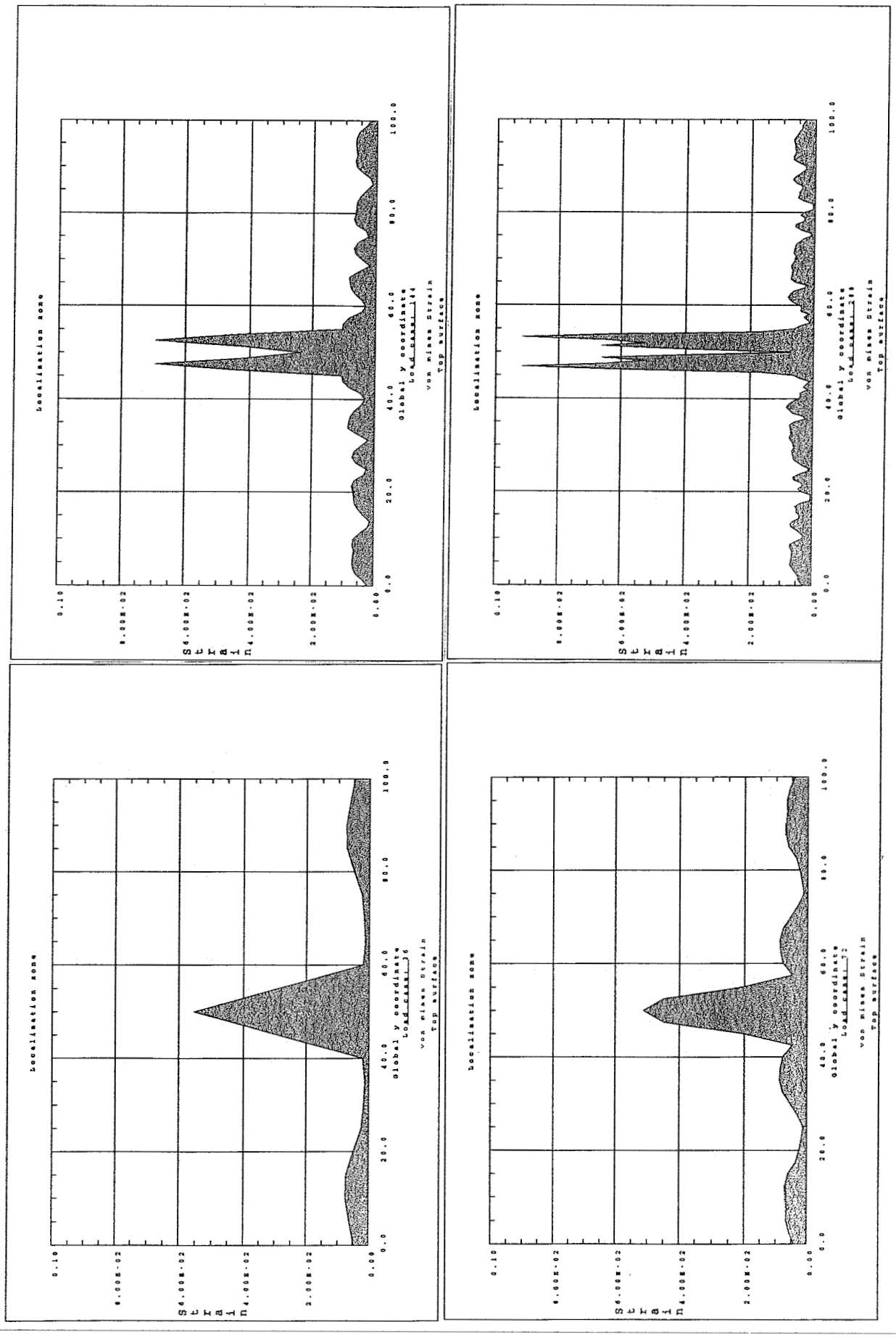

Fig 3.2.3. **Maximum principal strains at 36 μs - Shear model - viscous damage model : Coarse mesh (upper left corner) , Medium mesh (lower left corner), Fine mesh (upper right corner), Extra fine mesh (lower right corner)**

Results

All results are taken at time 36 μs, which corresponds with load step 36, 72, 144 and 288 for each mesh. At this time the shear wave has travelled trough 95 mm of the layer (50 mm elastically to the centre, 45 mm backwards to the boundaries). The results of the maximal principal strain distribution along the layer for the different meshes are given in figure 3.2.3. The corresponding deformed meshes in figure 3.2.4. show clearly the localisation zone. The global width of the localisation zone is almost identical for all meshes, but the fine meshes show two peaks indicating localisation in two symmetric integration points. Fig 3.2.5 illustrates the growth in time of these two peaks. The centre of the layer is unloading, (shear strain is decreasing in time), which might indicate that the localisation zone starts to propagate to the boundaries. In this sense, the results remain partially mesh-dependent. Another parameter-set can be chosen to avoid this problem. The analysis including viscoplasticity shows much better results on this topic.

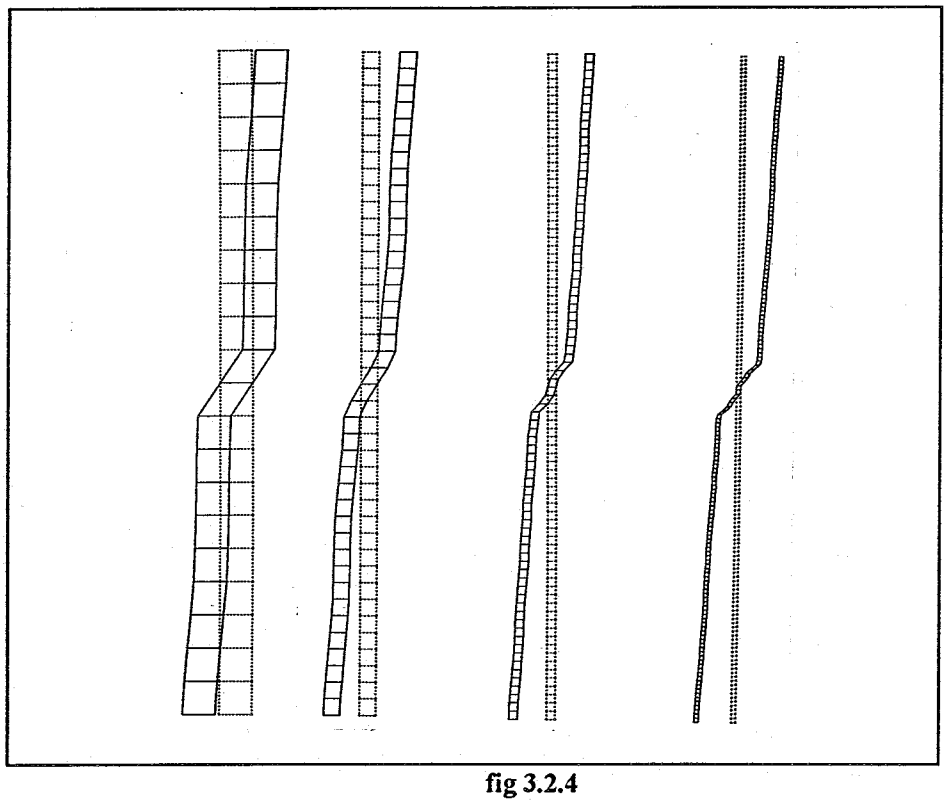

fig 3.2.4

The shear strain evolution in the layer is given in figure 3.2.5

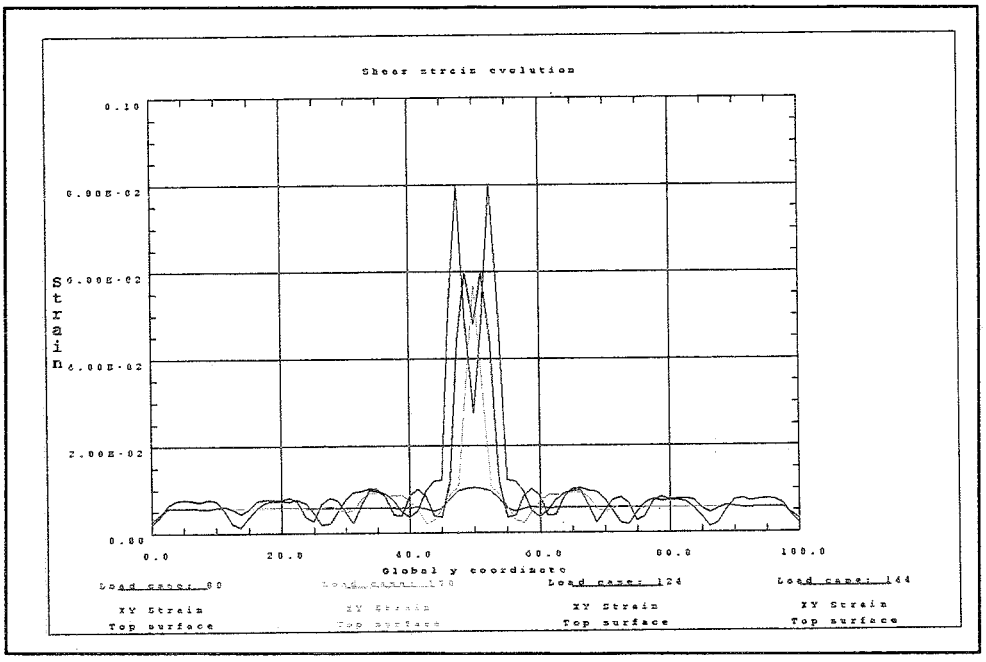

fig. 3.2.5.

3.2.3. Perzyna's viscoplastic - damage regularization

Model parameters

Damage : $K = 0{,}1\ MPa/s^{-2}$
$C = 1000\ s^{-1}$
$r = 2$
$D_c = 0.8$

Viscoplasticity : $\gamma = 30.\ s^{-1}$
$N = 2$
$\kappa = 100\,MPa$

The damage evolution law chosen for this analysis differs from the previous one by its tempered exponential character. Damage increase progresses more smoothly.

Results

Identically to the paragraph above, all results are taken at time 36 μs (load step 36, 72, 144 and 288). The results of the maximum principal strain distribution along the layer for the different meshes are given in figure 3.2.6. The corresponding deformed meshes in figure 3.2.7. show once more the localisation zone and the mesh-objective result that is obtained. The strain peaks for the fine and extra fine meshes are smaller than in the previous case. The better result is found with parameters that suit better the material behaviour. The deformed meshes no longer show the irregularities of figure 3.2.4. Again, we may conclude that Perzyna's viscoplastic model gives a smoother local result then the viscous damage approach alone.

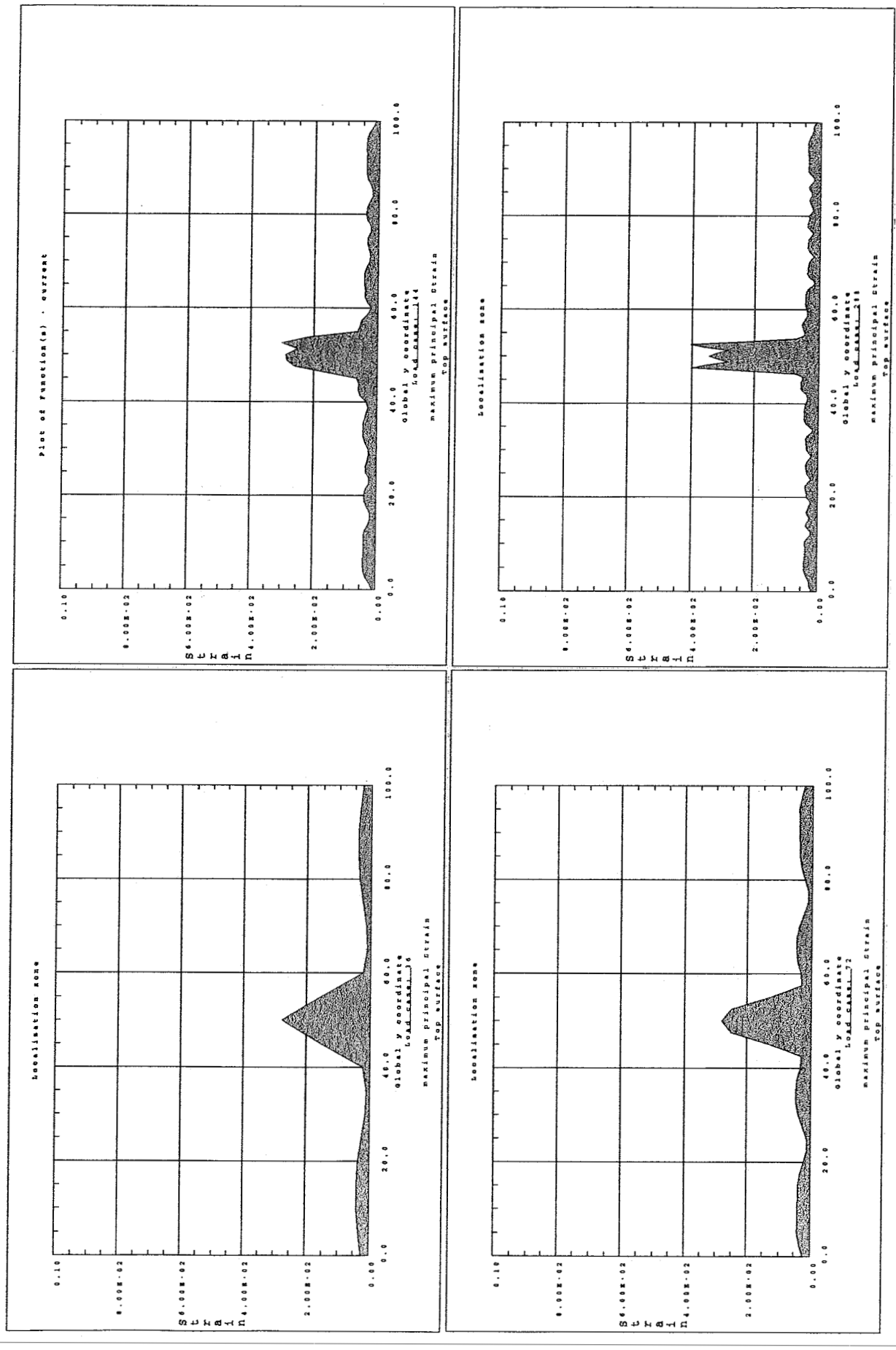

Fig 3.2.6. Maximum principal strains at 36 μs - Shear model - Perzyna's viscoplasticity involving damage : Coarse mesh (upper left corner) , Medium mesh (lower left corner), Fine mesh (upper right corner), Extra fine mesh (lower right corner)

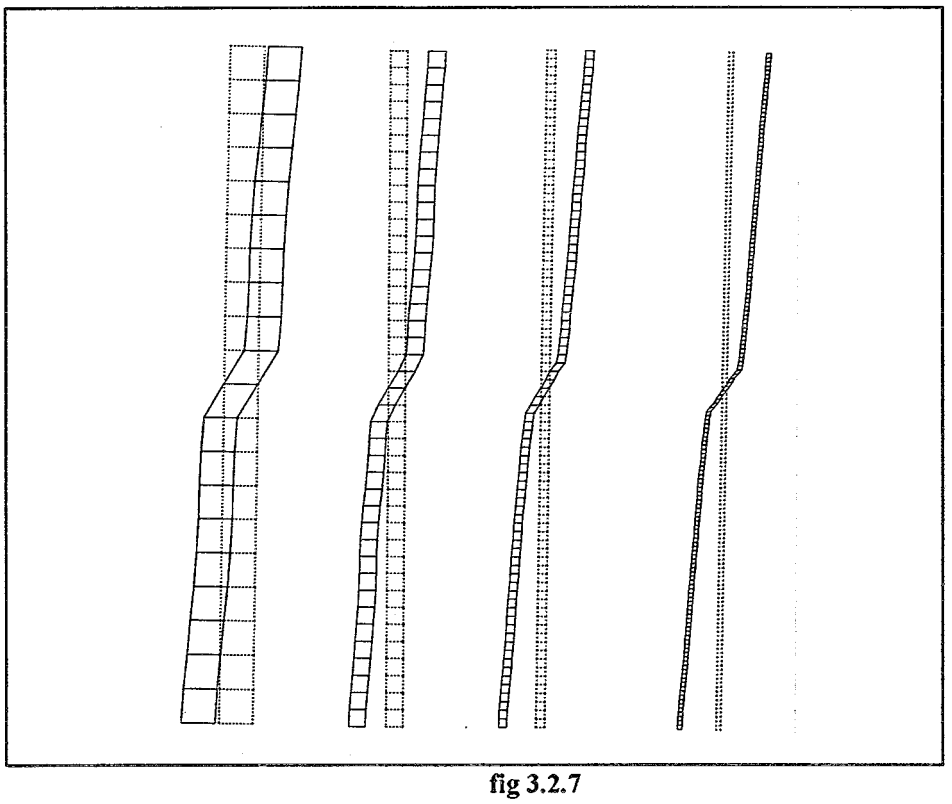

fig 3.2.7

It appears that viscous regularization (damage and viscoplasticity) is a very useful numerical tool in dynamic problems (significant strain rates). The shear strain evolution in the layer is given in figure 3.2.8 below.

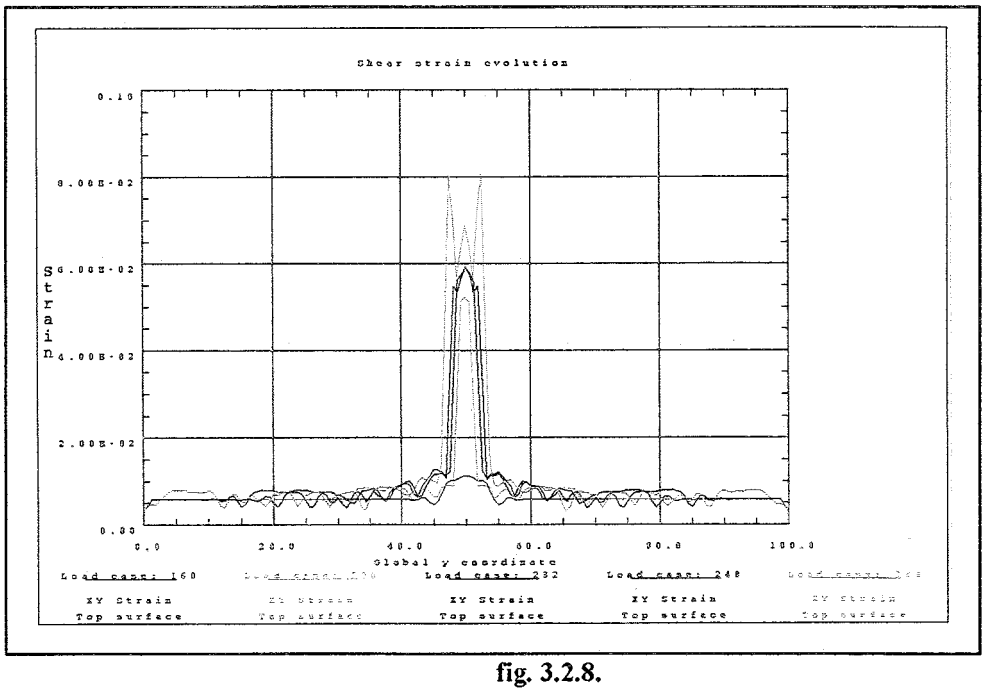

fig. 3.2.8.

It is important to remark that the mesh-objectivity depends on the viscous character that is attributed to the viscoplastic model or the damage evolution law. Another choice for the numerical parameters leads to other results. This is shown in figure 3.2.9. where no localisation was found in the first case and a very narrow localisation-band in the second case. The numerical values should be chosen appropriate to the material and the applied load. In this analysis all parameters were fitted to control the localisation time. Modification of the parameters results in a different localisation-width with possibly different localisation-times.

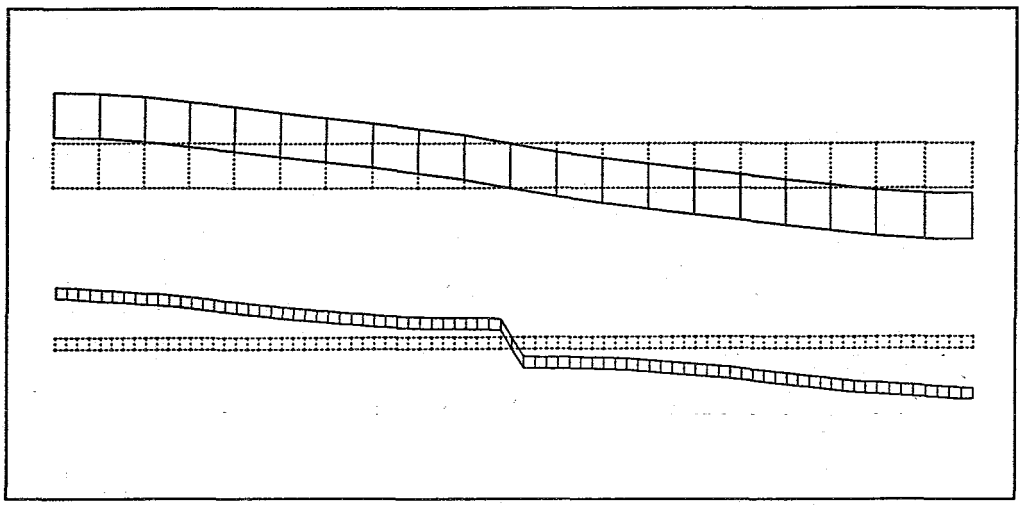

fig. 3.2.9.

4. Conclusions

The results from the present study confirm the regularizing capacities of viscous models in localisation by strain-softening. Comparisons with other studies using a strain-softening function instead of damage are not as evident as they seem. Models using a strain-softening function need to be coupled to a constitutive model to operate correctly (by relating the rate of the hardening/softening parameter to the viscoplastic strain rate). A damage model with a viscous behaviour is capable to ensure dynamic regularization of strain localisation itself. The viscoplastic component in the combined constitutive model permits to do the fine-tuning and offers a broad range of possible numerical parameters to fit calculations to experiments.

Most of the conclusions have been made while discussing the results. What is essential can be summarised as follows :

1. A viscous damage approach permits to regularise the strain localisation for strain softening materials. An adequate parameter set should be used to fit on reality.
2. The combination of a viscous damage evolution law and Perzyna's viscoplastic model leads to mesh-objective results if parameters are well chosen. Strains are smoother distributed in the localisation zone.
3. Viscous regularization is useful for dynamic and quasi-static problems. All parameters are rate-dependent and should be adapted to the rate or frequencies of the applied load.
4. Conclusions towards the merits of a regularizing constitutive model, must be made with care. The failure criterion fully determines whether mesh-insensitivity is ensured or not. If the analysis is carried out long enough, damage will always exceed the critical value on integration point level (thus mesh-dependent). The viscous regularization delays this inherent mesh-independence and widens the localisation zone. If failure occurs before the viscous model loses mesh-insensitivity, the model satisfies for that particular failure criterion.
5. Although results may satisfy globally, some small local differences will always remain between the meshes. Some of these differences still arise from a local mesh-dependence, but others may simply result from the convergence to the exact solution.

References

BORST, R. de and MUHLHAUS, H.-B. (1991) - 'Computational strategies for gradient continuum models with a view to localisation of deformation', *Proc. 4th. Int. Conf. on Non-linear Eng. Comp.*, Eds. N. Bicanic, P. Marovic, D.R.J. Owen, V. Jovic and A. Mihanovic, Pineridge Press, Swansea, pp. 239-260.

BORST, R. de, MUHLHAUS, H.-B., PAMIN, J. and SLUYS, L.J. (1992) - 'Computational modelling of localisation of deformation', *Proc. Conf. on Computational Plasticity, Fundamentals and Applications, Part II,* Eds. D.R.J. Owen, E. Oñate and E. Hinton, Pineridge Press, Swansea, pp. 483-508.

BREKELMANS; W.A.M. (1993) - 'Nonlocal formulation of the evolution of damage in a one-dimensional configuration' *Int. J. Solids Structures* ,**30** ,pp. 1503-1512.

HUGHES, T.J.R. (1987) - *The finite element method - Linear static and dynamic finite element analysis,* Prentice-Hall, New Jersey

KACHANOV, L.M. (1986) - *Introduction to Continuum Damage Mechanics.* Martinus Nijhoff Publishers, Dordrecht.

LEMAITRE, J. and CHABOCHE, J.-L. (1990) - *Mechanics of Solid Materials.* Cambridge University Press, Cambridge.

NEEDLEMAN, A. (1988) - Material rate dependence and mesh sensitivity in localisation problems. *Comp. Meth. Appl. Mech. Eng.*, **67**, pp.68-85

PERZYNA, P. (1966) - 'Fundamental problems in viscoplasticity', *Recent Advances in Applied Mechanics,* Academic Press, New York, **9**, pp. 243-377.

PERZYNA, P. (1971) - Thermodynamic theory of viscoplasticity. *Advances in Applied Mechanics,* Academic Press, New York, **11**.

SIMO, J.C. (1988) - 'Strain softening and dissipation : a unification of approaches.' *Cracking and Damage, Strain Localisation and Size effects,* J. Mazars and Z.P. Bazant eds, Elsevier Applied Science, London, pp. 440-461.

SLUYS, L.J. (1992) - *Wave propagation, Localisation and dispersion in softening solids,* Graduation thesis, Delft University of Technology, Delft.

TIMMERMANS, P.H.M. BREKELMANS, W.A.M., VREE, J.H.P. de (1992) - *Phenomenological modelling of damage in polymer blends,* Dissertation, Eindhoven University of Technology, Eindhoven.

ZIENKIEWICZ O.C., TAYLOR R.L. (1989) - *The Finite Element Method - 4th ed.*, Mc Graw-Hill